Assessments of ATMS and SSMIS Data for NWP Applications

Fuzhong Weng
JCSDA Senior Scientist
Satellite Meteorology and Climatology Division
NOAA/NESDIS/Center for Satellite Applications and Research

JCSDA Seminar, June 20, 2012

Outline

- **Current Observing System for NWP**
  - Data used in GFS
  - Impacts from uses of satellite data
  - Optimal global observing system
- **Microwave Sounding Systems – Conical vs Cross-Track**
  - Pros and Cons
  - Convertibility issue of TDR to SDR
  - Changing practices in forward model
- **Assessments of Instrument Performance wrt NWP**
  - Cloud algorithm for NWP control controls
  - ATMS sounding channels
  - SSMIS sounding Channels
- **Summary and Conclusions**

US Current Polar Satellite System Program

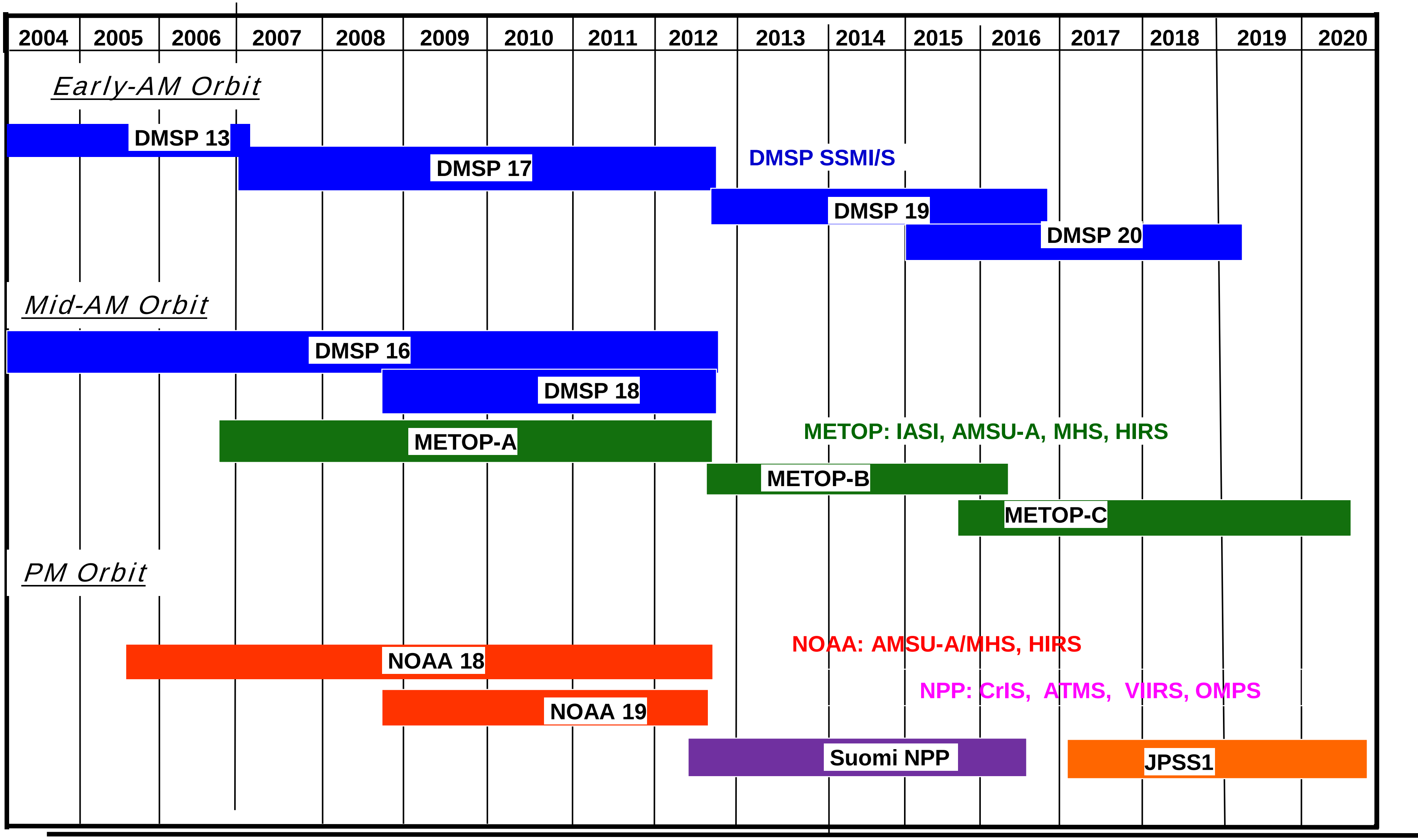

JPSS Era System

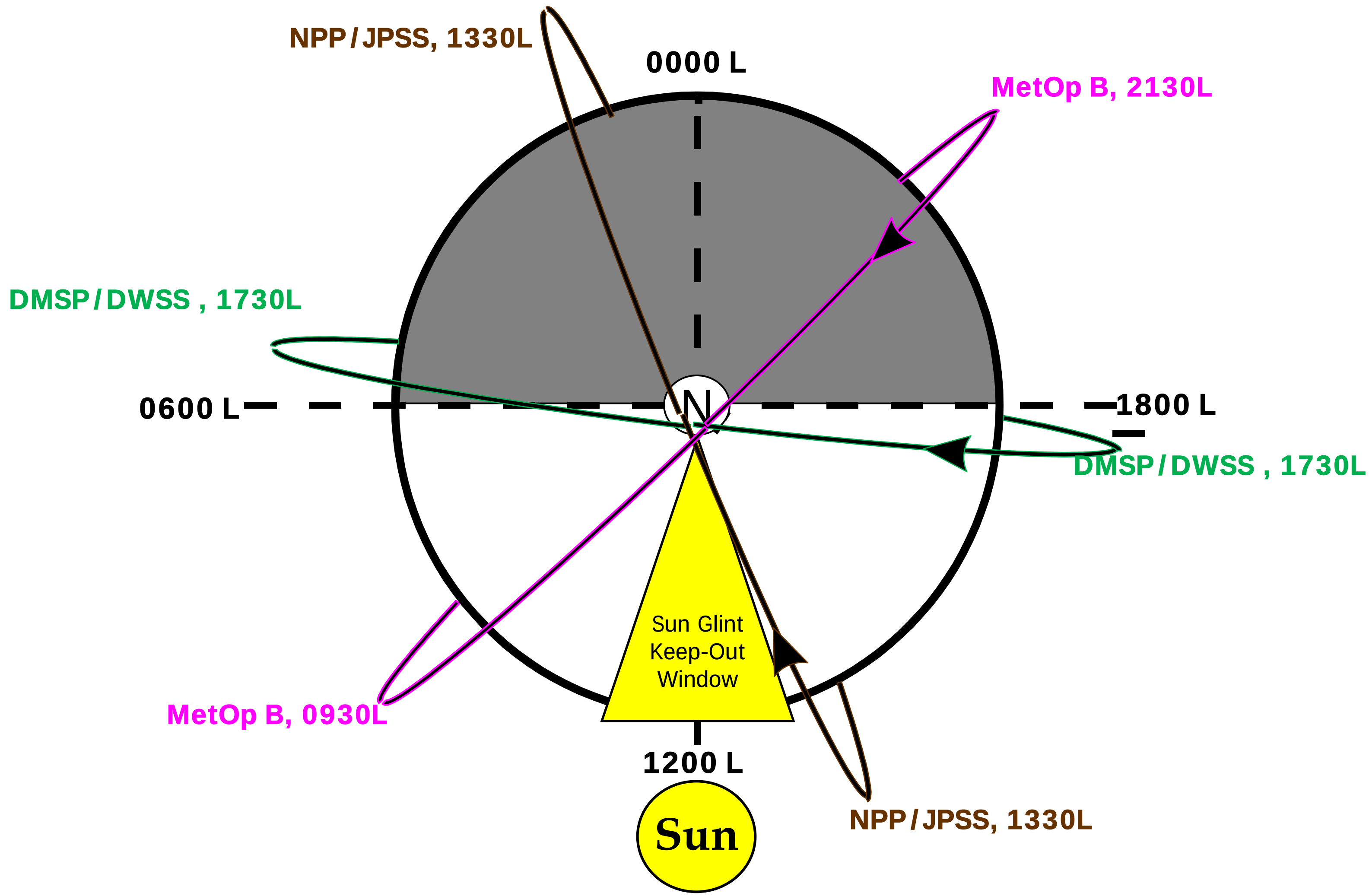

JPSS will Extend and Replace the Heritage NOAA Satellites that are Crucial to National Operational Capabilities of both NOAA and DoD

Impacts of Satellite/Conventional Data on Global Forecast Model

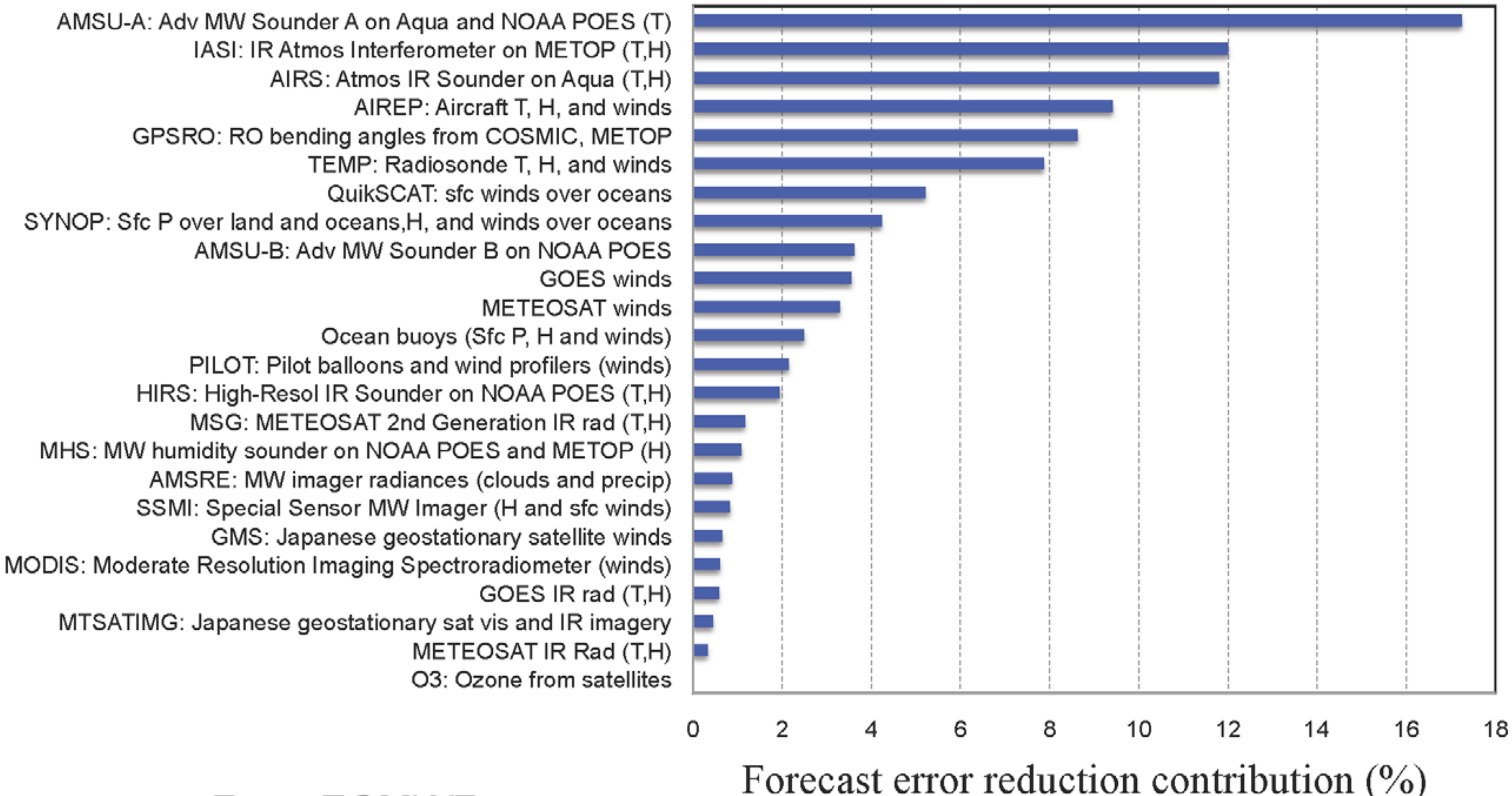

From ECMWF

Impacts from assimilation of satellite data on NWP forecasts are larger than those from conventional data. Much of the impacts is attributed to use of microwave/IR/GPSRO sounding data

Atmospheric Transmission at Microwave Wavelengths

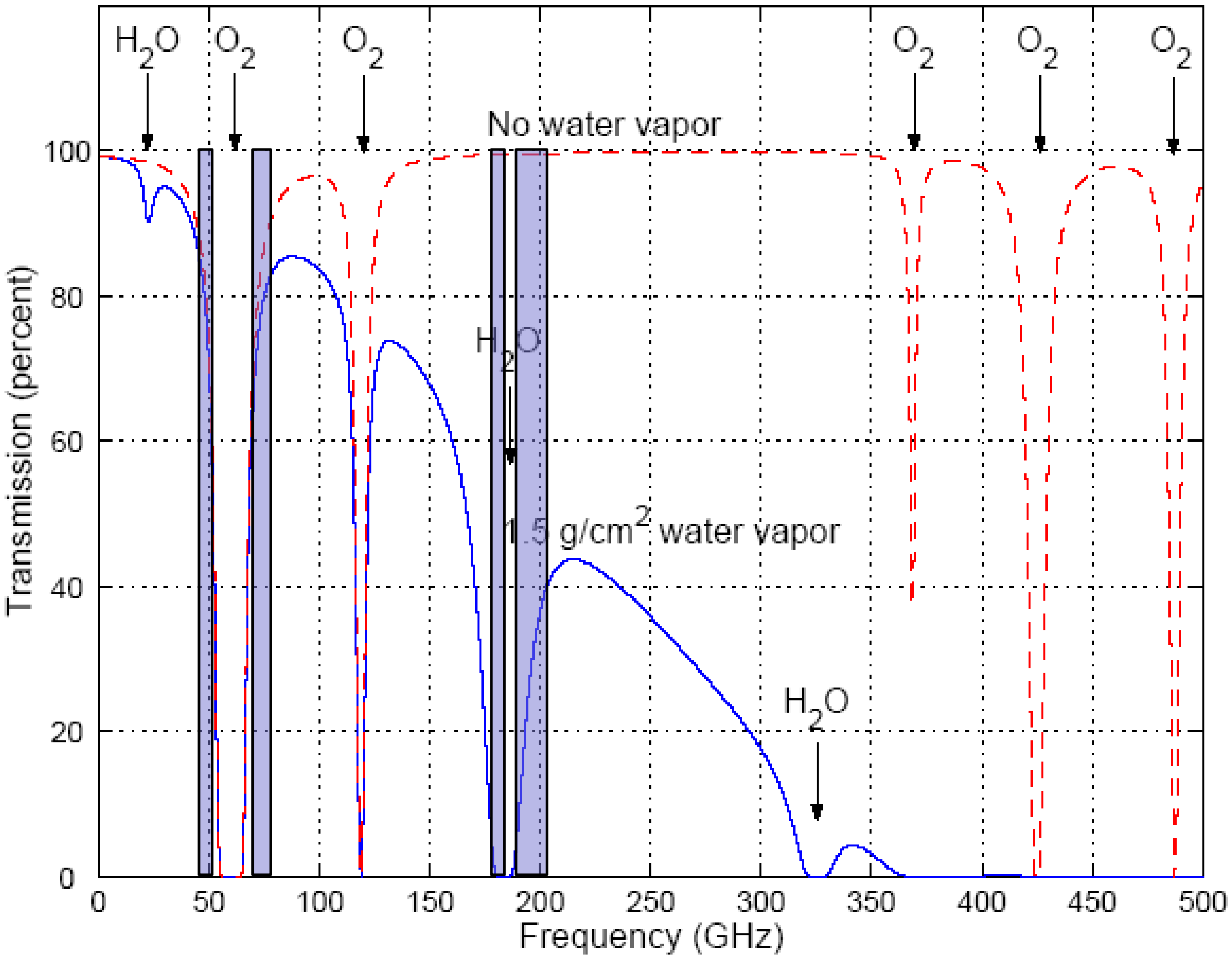

The frequency dependence of atmospheric absorption allows different altitudes to be sensed by spacing channels along different absorption lines.

Microwave Temperature Sounding Vertical Resolution

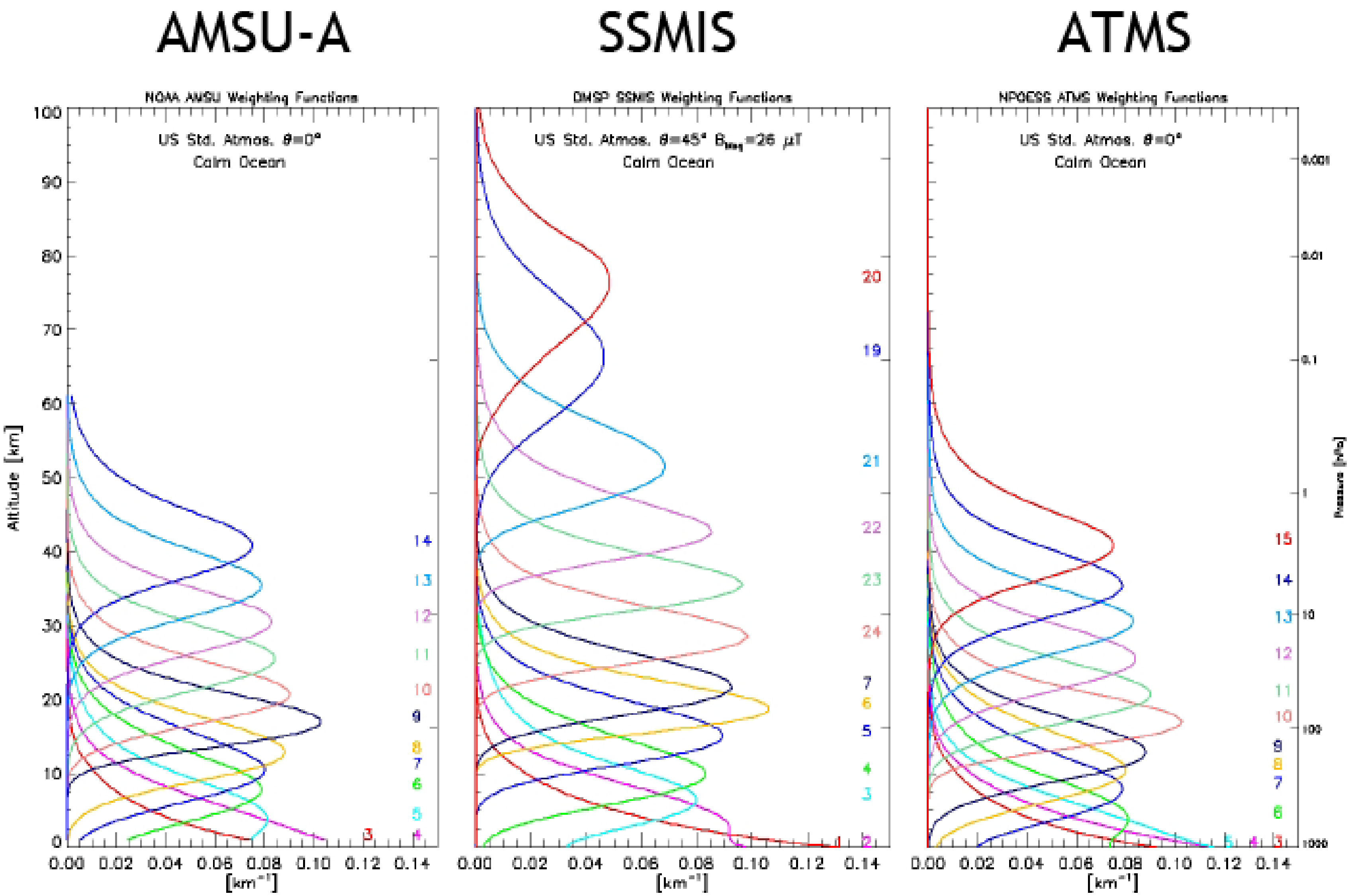

Conical vs Cross Track Sounding

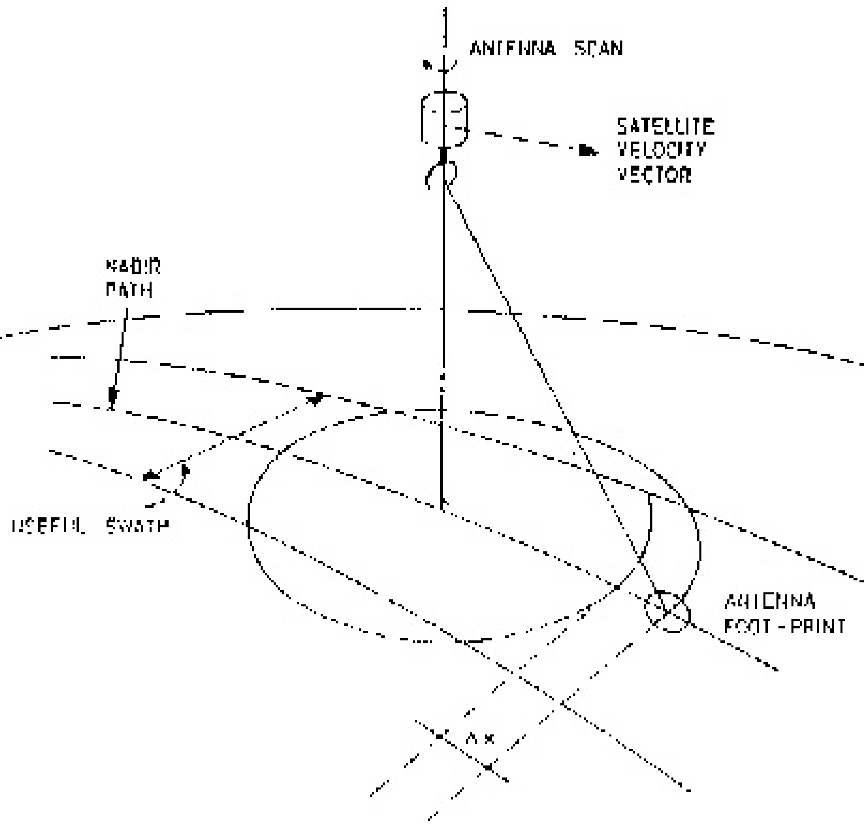

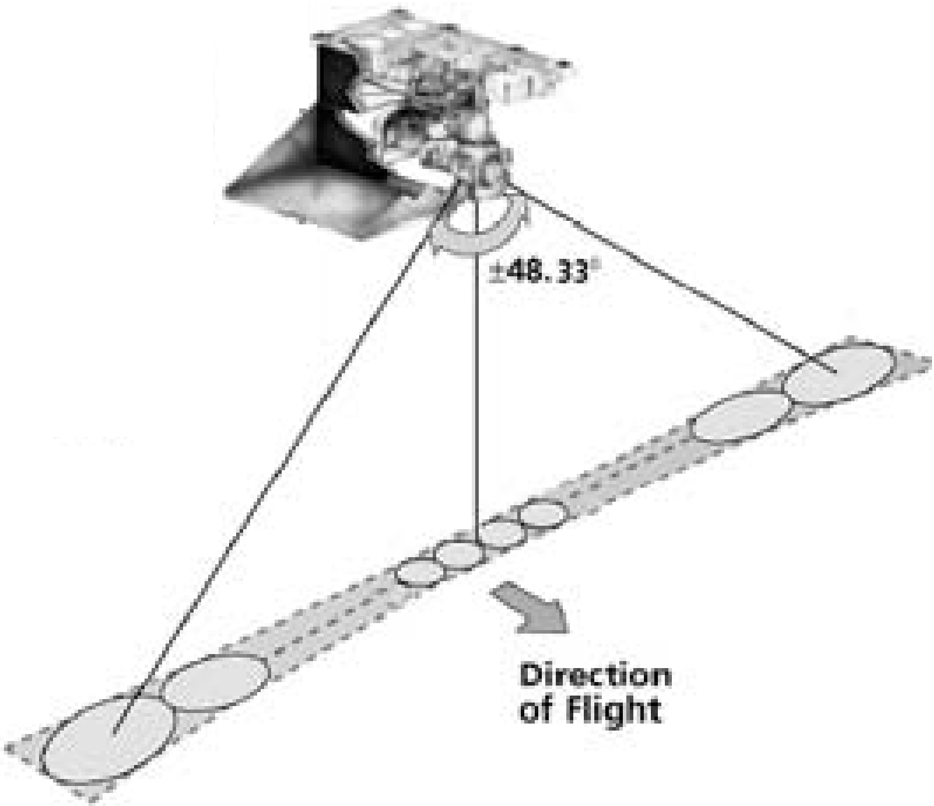

- Narrow scan swath width with orbit gap
- FOV size is the same for all positions but varies with frequencies
- Same pol for all scan positions

- Large scan swath width (no orbit gap)
- Same resolution for all frequencies
- Mixing pol as scan from nadir to limb
- Res varies with scan angle

Suomi NPP Spacecraft and Payloads

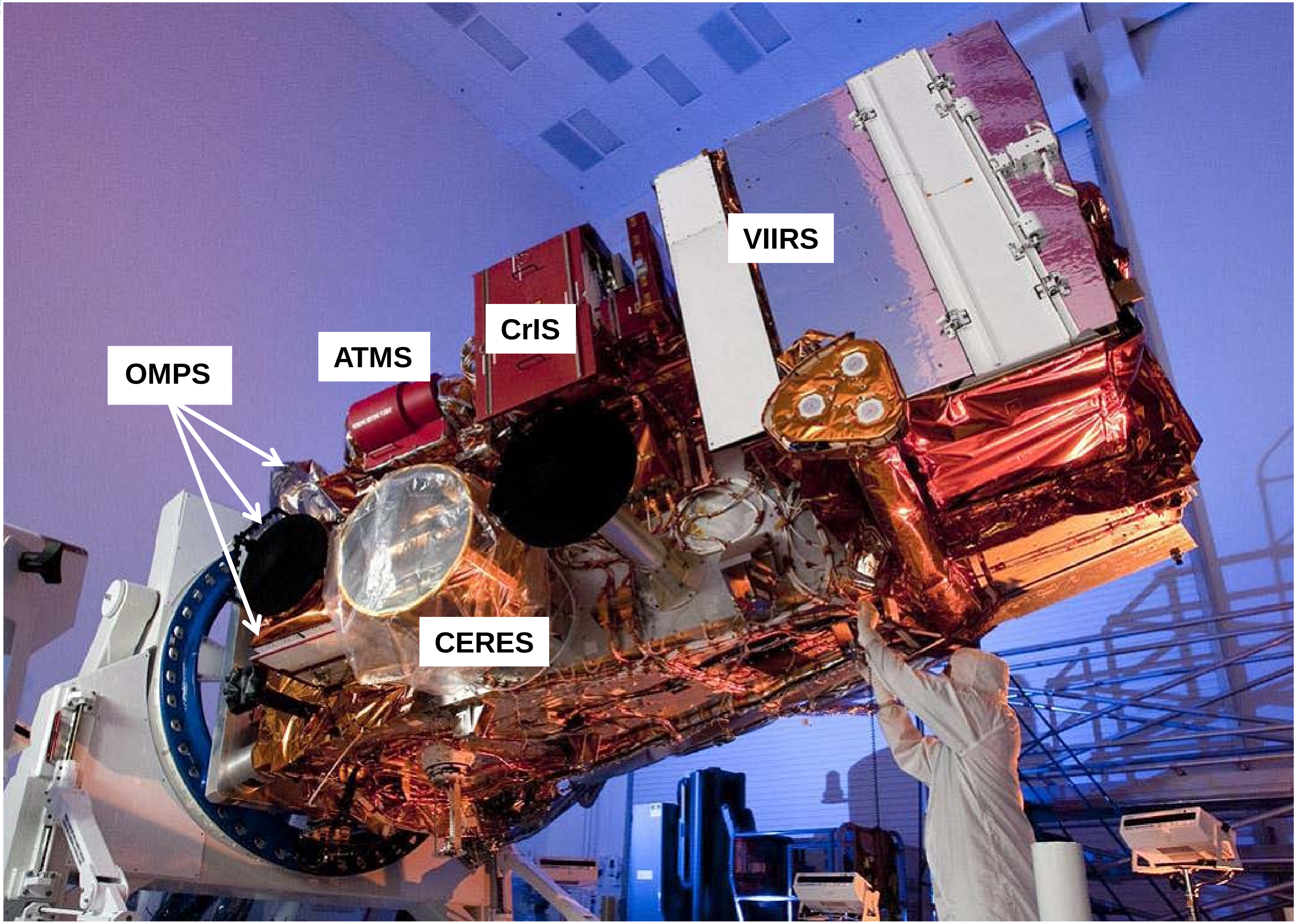

ATMS after Assembly

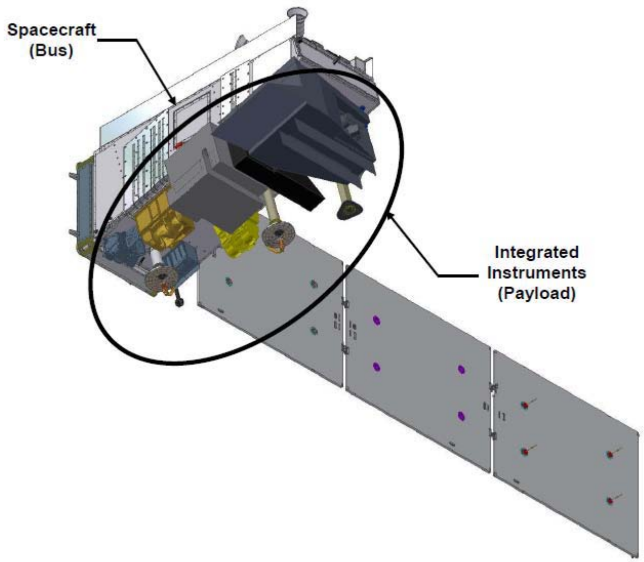

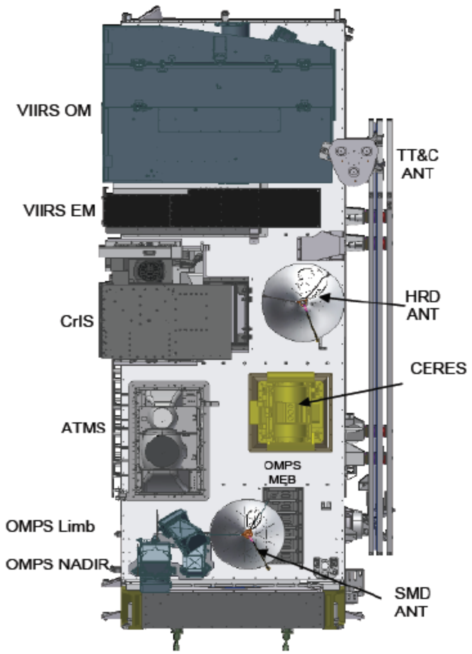

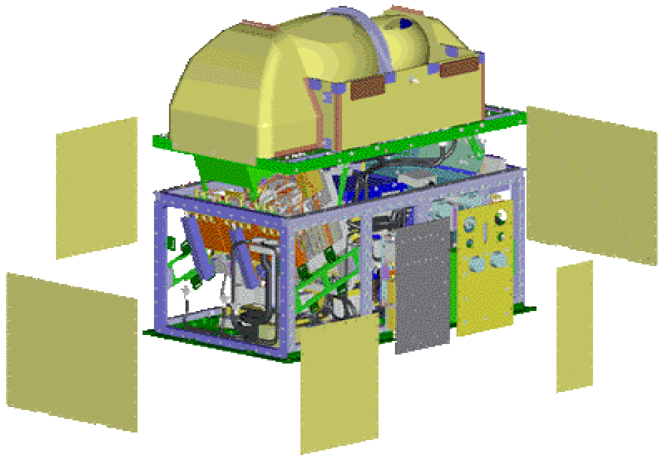

– 70x40x60 cm

– 110 W

– 85 kg

– 8 year life

ATMS Scanning Assembly

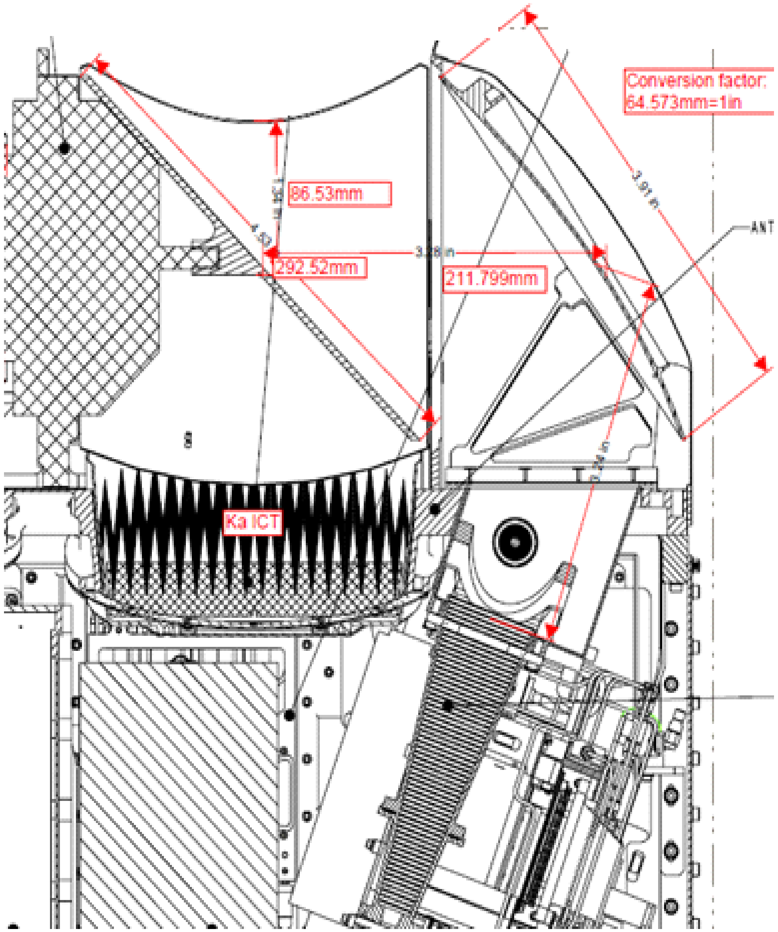

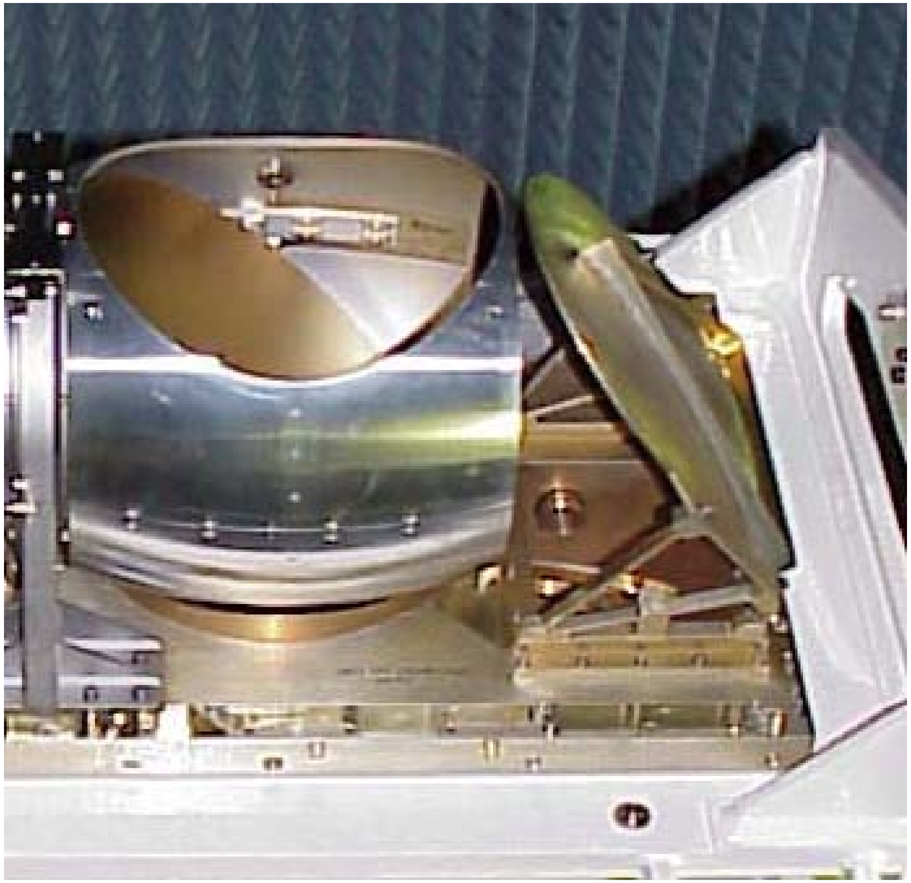

Courtesy of NGES

Channel Characteristics of ATMS and AMSU

Channel		Frequency (GHz)		NEΔT (K)		Beam width (°)		Peak WF (hPa)	
ATMS	AMSU	ATMS	AMSU	ATMS	AMSU	ATMS	AMSU	ATMS	AMSU
1		23.8		0.50	0.30	5.2	3.3	Surface	
2		31.4	31.399	0.60	0.30	5.2	3.3	Surface	
3		50.3	50.299	0.70	0.40	2.2	3.3	Surface	
4		51.76		0.50		2.2		Surface	
5	4	52.8		0.50	0.25	2.2	3.3	1000	
6	5	53.596±0.115		0.50	0.25	2.2	3.3	700	
7	6	54.4		0.50	0.25	2.2	3.3	400	
8	7	54.94		0.50	0.25	2.2	3.3	270	
9	8	55.5		0.50	0.25	2.2	3.3	180	
10	9	57.29		0.75	0.25	2.2	3.3	90	
11	10	57.29± 0.217		1.00	0.40	2.2	3.3	50	
12	11	57.29± 0.322± 0.048		1.00	0.40	2.2	3.3	25	
13	12	57.29± 0.322 ± 0.022		1.25	0.60	2.2	3.3	12	
14	13	57.29± 0.322 ± 0.010		2.20	0.80	2.2	3.3	5	
15	14	57.29± 0.322± 0.0045		3.60	1.20	2.2	3.3	2	
16	15	88.2	89.0	0.30	0.50	2.2	3.3	Surface	
17	16	165.5	89.0	0.60	0.84	1.1	1.1	1000	Surface
18	17	183.31±7.0	157.0	0.80	0.84	1.1	1.1	800	Surface
19	18	183.31±4.5	183.31±1.0	0.80	0.60	1.1	1.1	700	400
20	19	183.31±3.0		0.80	0.70	1.1	1.1	600	
21	20	183.31±1.8	183.31±7.0	0.80	1.06	1.1	1.1	500	800

ATMS Scan Angle and Beam Width

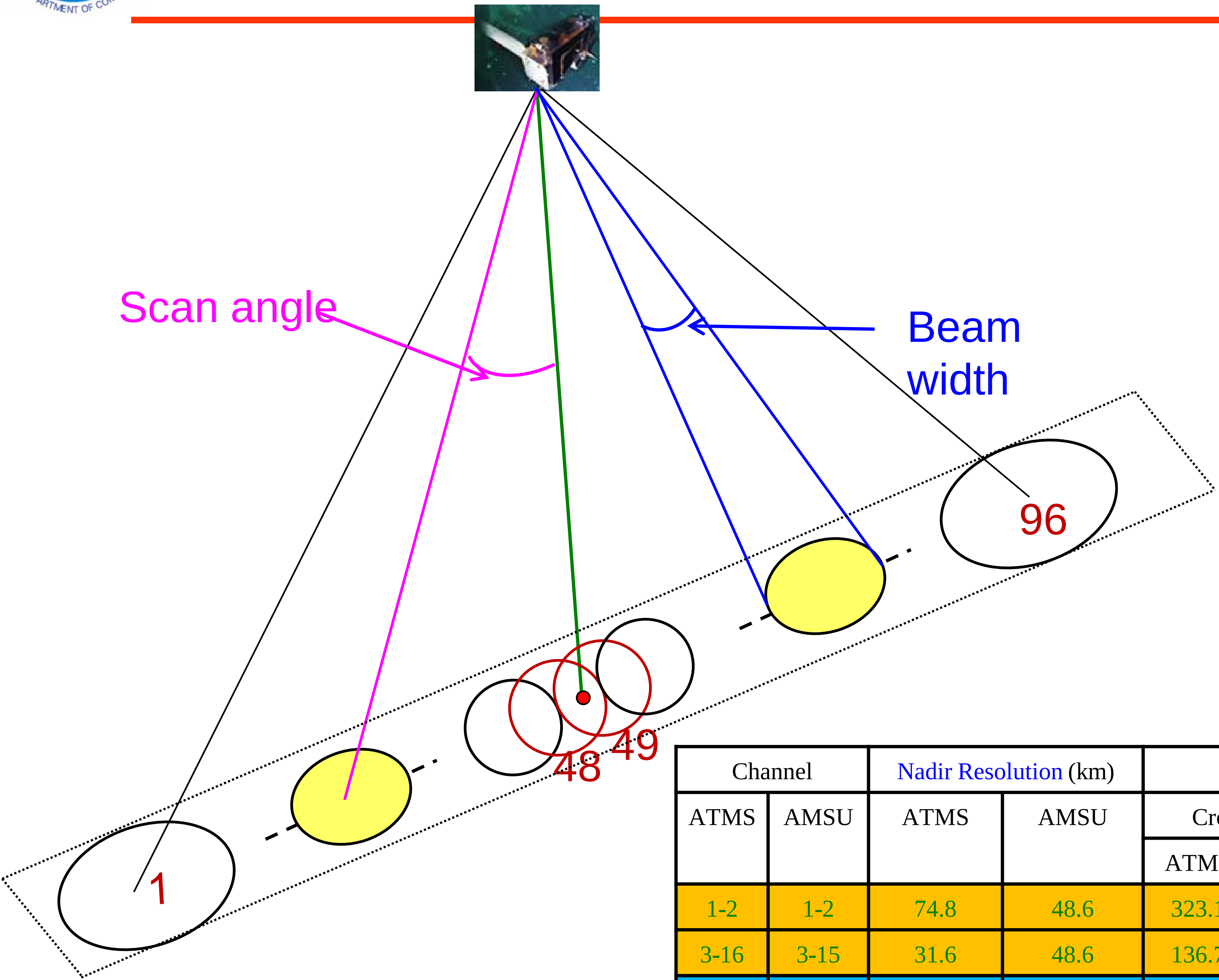

Channel		Nadir Resolution (km)		Outmost FOV size (km)			
ATMS	AMSU	ATMS	AMSU	Cross-track		Along-track	
				ATMS	AMSU	ATMS	AMSU
1-2	1-2	74.8	48.6	323.1	155.2	141.8	85.6
3-16	3-15	31.6	48.6	136.7	155.2	60.0	85.6
17-22	16-20	15.8	16.2	68.4	58.9	30.0	29.4

Spatial Differences: ATMS vs. AMSU/MHS

Beamwidth (degrees)

	ATMS	AMSU/MHS
23/31 GHz	5.2	3.3
50-60 GHz	2.2	3.3
89-GHz	2.2	1.1
160-183 GHz	1.1	1.1

Spatial sampling

	ATMS	AMSU/MHS
23/31 GHz	1.11	3.33
50-60 GHz	1.11	3.33
89-GHz	1.11	1.11
160-183 GHz	1.11	1.11
Swath (km)	~2600	~2200

ATMS scan period: 8/3 sec; AMSU-A scan period: 8 sec

Impacts of ATMS Spatial Re-sampling on NWP O-B

ATMS Field of View Size for the beam width of 2.2º – black line

ATMS Resample to the Field of View Size for the beam width of 3.3º- blue line

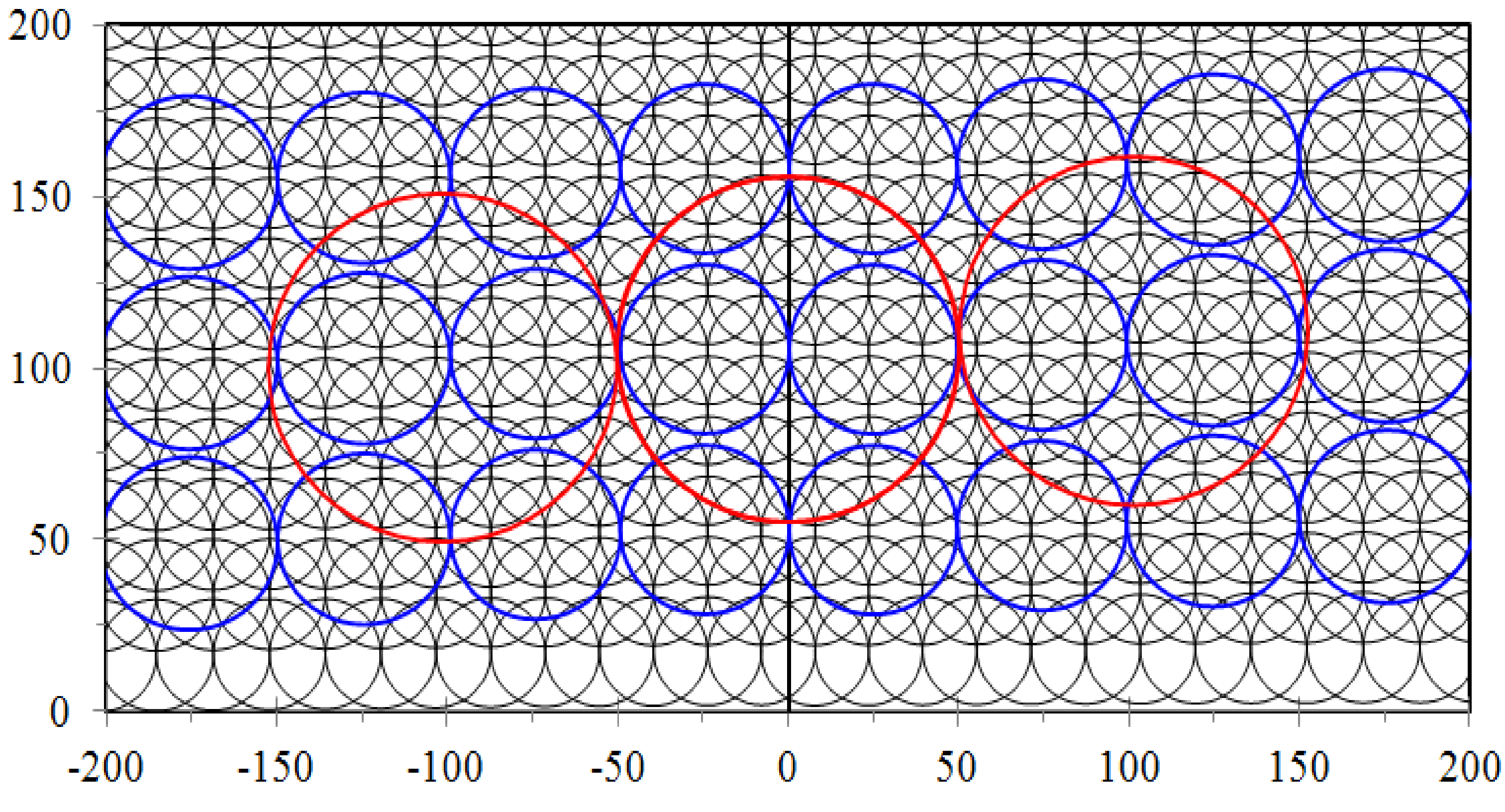

ATMS CalVal Status

- Beta version of ATMS TDR data was declared on February 22, 2012
  - ATMS instrument noises (NEDT) are characterized and all channels meet the requirements
  - Onboard calibrators are functioning normally and stable, providing good quality data for TDR calibration
  - Cold space calibration profile one is selected for ATMS calibration
- Provisional version of ATMS TDR has been achieved in May, 2012
  - Accuracy of ATMS sounding channels is characterized with GPSRO data and within 1.0-2.0 K
  - Effects of ATMS spectral response function are investigated and the improvements for forward modeling are significant (up to 0.2 to 0.3K)

ATMS Channel NEΔT

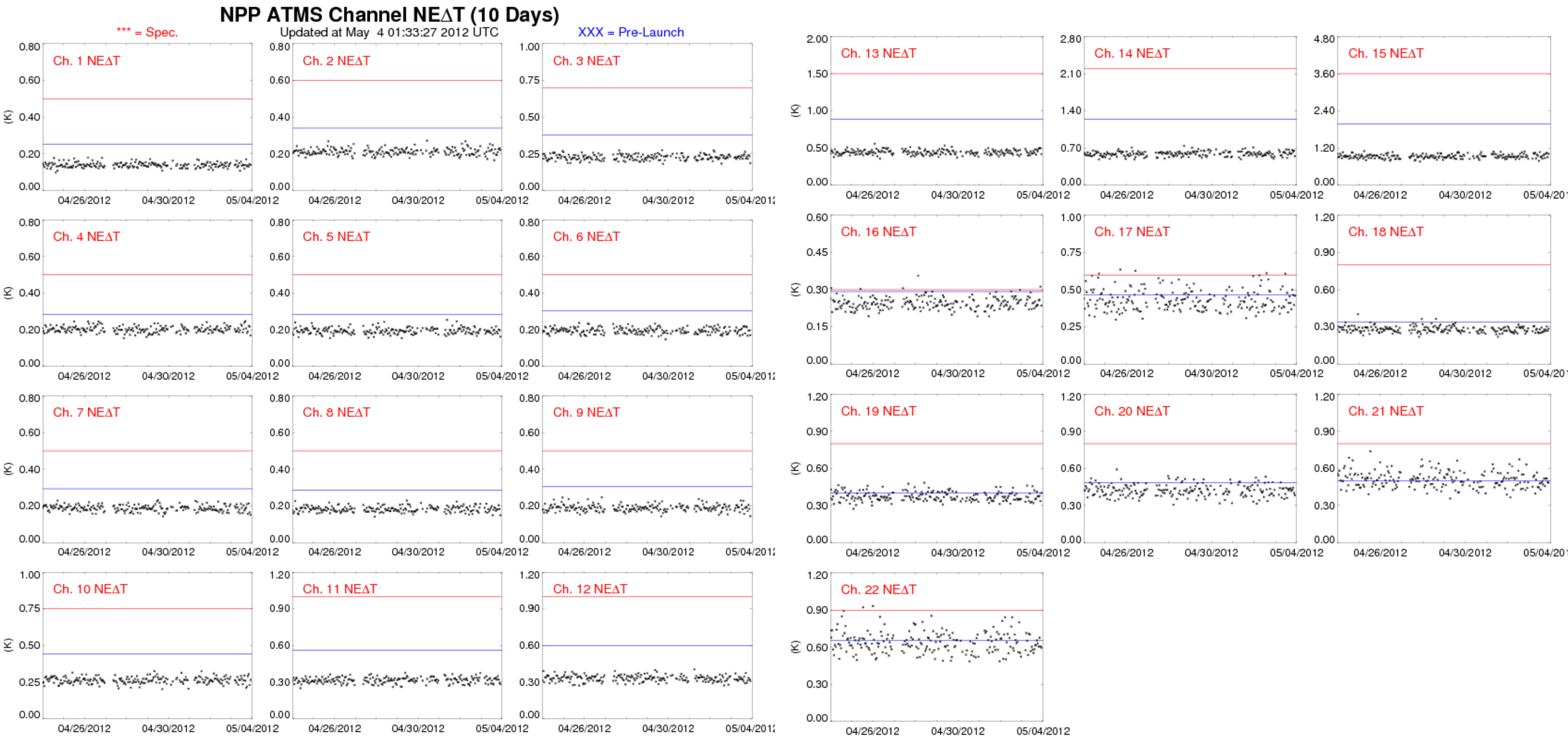

NPP ATMS on-orbit NEΔT (black) are within specifications (red)

ATMS Space View Count

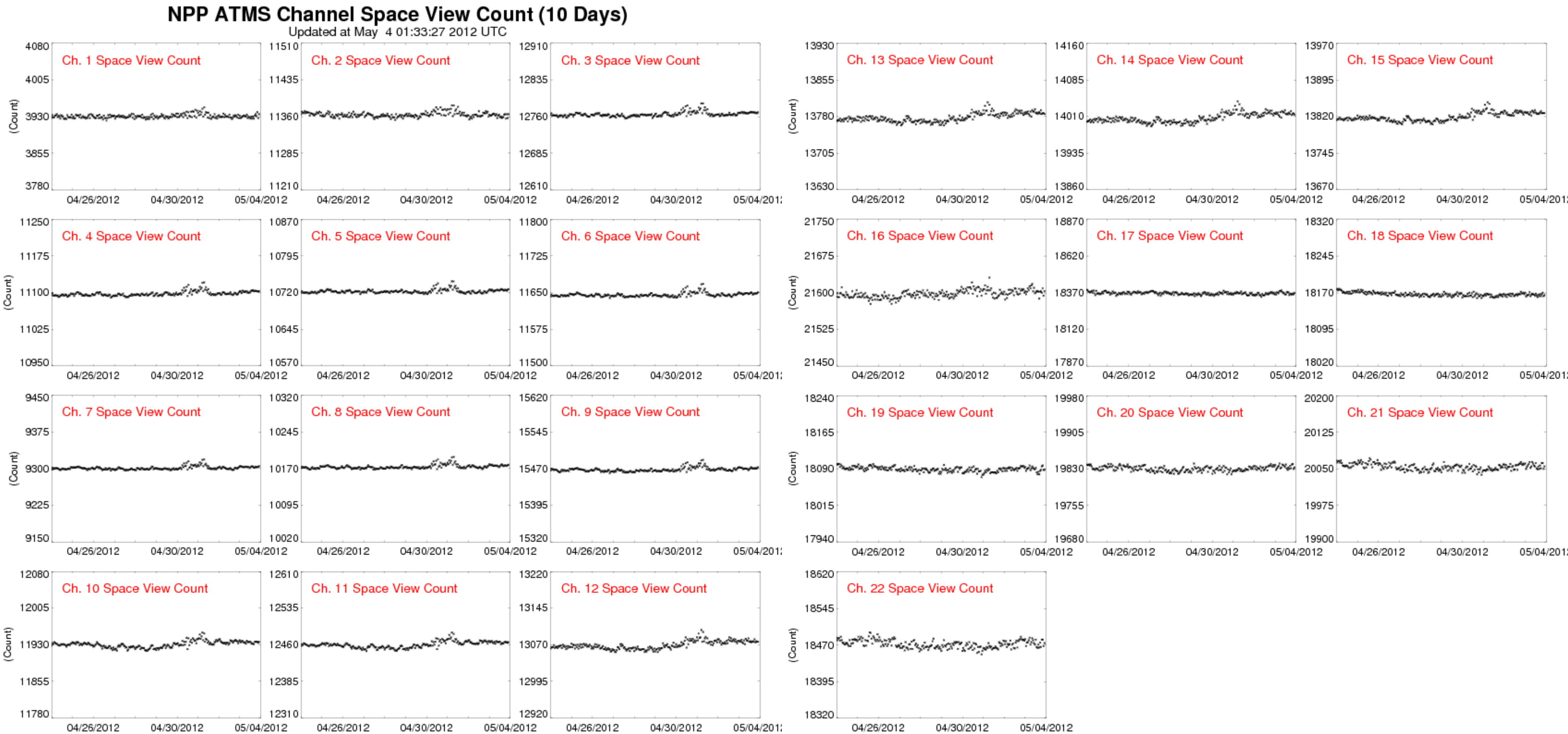

- NPP ATMS space view calibration counts are stable
- NPP ATMS warm load calibration counts and gain are also stable (not shown)

K/Ka Band 4-Wire PRT Temperature

- K/Ka band 4-wire warm load PRT temperature (8 readings) is stable
- W/G band 4-wire warm load PRT temperature (7 readings) is stable too (not shown)

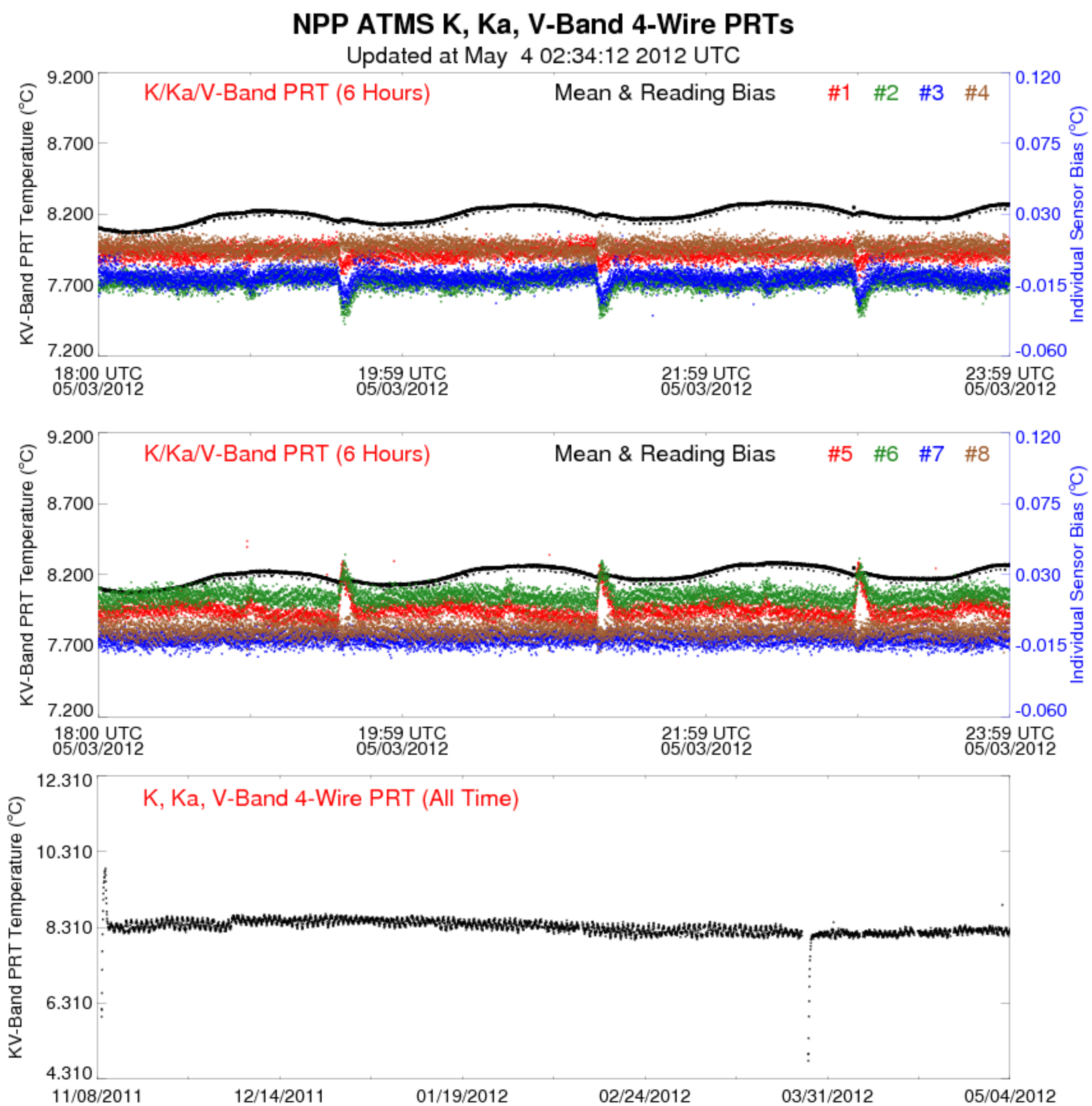

ATMS Noise Equivalent Differential Temperature (NEDT)

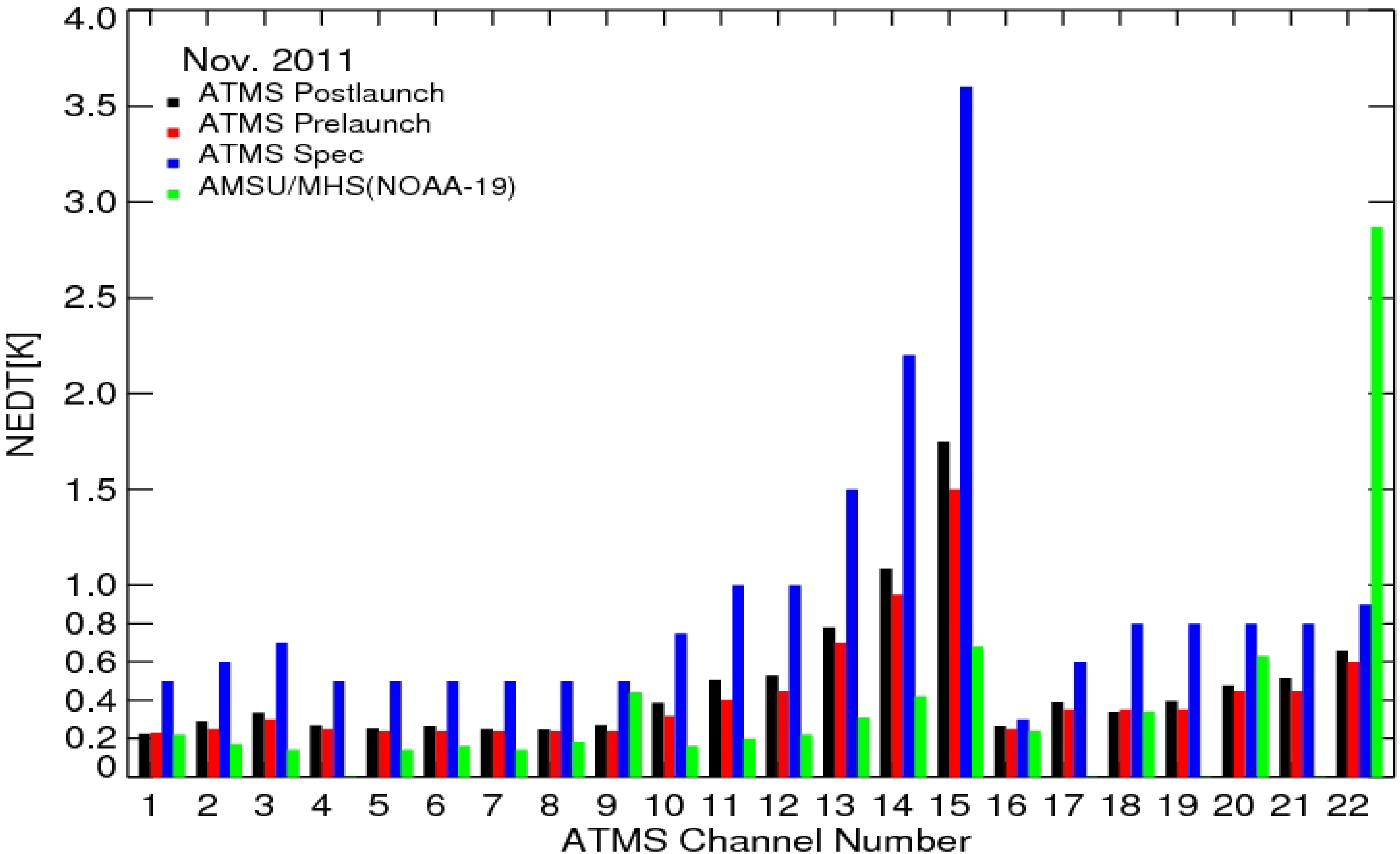

Assessments of ATMS Performance Using NWP O-B

Approach 1: no antenna models applied for observations or simulations

Observation (O): Antenna brightness temperature (TDR) from satellite observations

Background (B): Simulated brightness temperature (SDR) from NWP forecast fields or other profiles

Approach 2: Antenna models for converting TDR to SDR

Observation (O): Sensor brightness temperature (SDR) from satellite observations.

Background (B): Simulated brightness temperature (SDR) from NWP forecast fields or other profiles

Approach 3 : Antenna model applied for converting simulated SDR to TDR

Observation (O): Antenna brightness temperature (TDR) from satellite observations

Background (B): Simulated antenna brightness temperature (TDR) from NWP forecast fields or other profiles

Antenna/Sensor Brightness Temperature for Cross-Track Scanning Instrument

SDR

TDR

$$T_a^{Qv} = \eta_{me}^{vv} T_b^{Qv} + \eta_{me}^{hv} T_b^{Qh} + \eta_{se}^{vv} E_b^{Qv} + \eta_{se}^{hv} E_b^{Qh} + \eta_{sc}^{vv} C_b^{Qv} + \eta_{sc}^{hv} C_b^{Qh} + S_a^{Qv}$$

SDR

$$T_a^{Qh} = \eta_{me}^{hh} T_b^{Qh} + \eta_{me}^{vh} T_b^{Qv} + \eta_{se}^{hh} E_b^{Qh} + \eta_{se}^{vh} E_b^{Qv} + \eta_{sc}^{hh} C_b^{Qh} + \eta_{sc}^{vh} C_b^{Qv} + S_a^{Qv}$$

The first two terms are Quasi-V and Quasi-H brightness temperature from earth in the main beam (main lobe earth), the 3rd/4th terms are those from the side-lobe earth, the 5/6th terms are side-lobe cold space,, the last two are near-field satellite radiation. Specifically

$$T_b^{Qv} = T_b^v \cos^2\theta + T_b^h \sin^2\theta \qquad T_b^{Qh} = T_b^v \sin^2\theta + T_b^h \cos^2\theta$$

Under a polarized earth scene, the cross-polarization term can result in large errors in computing SDR from TDR data if the antenna has a significant spill-over effect and the cross-polarization term is neglected.

Convertibility Issues from TDR to SDR

- Need to correct side-lobe radiation from far-field earth and near-field satellites

- For a sensor with a significant cross-polarization spill-over, an inversion from TDR to SDR is problematic if a single polarization measurement is provided

- For un-polarized surface and atmospheric conditions, the inversion from TDR to SDR is possible with a single polarization measurement.

ATMS Antenna Beam Efficiency

Frequency (GHz)	η_{me}^{pp} (%)			η_{me}^{pq} (%)			$\eta_{se}^{pp}+\eta_{sc}^{pp}+\eta_{ss}^{pp}$ (%)		
	B1	B48	B96	B01	B48	B96	B01	B48	B96
23.8	99.48	99.61	99.53	0.52	0.39	0.46	0.003	0.0002	0.0025
31.4	99.59	99.60	99.60	0.40	0.40	0.39	0.003	0.0003	0.0024
50.3	99.43	99.39	99.56	0.57	0.61	0.44	0.001	0.0006	0.0008
51.8	99.45	99.47	99.73	0.55	0.53	0.27	0.001	0.0004	0.0007
52.8	99.48	99.46	99.36	0.51	0.54	0.64	0.001	0.0004	0.0010
53.6	99.49	99.43	99.31	0.51	0.57	0.68	0.001	0.0004	0.0008
54.4	99.51	99.51	99.55	0.49	0.49	0.44	0.001	0.0006	0.0006
54.9	99.48	99.49	99.21	0.51	0.51	0.78	0.001	0.0004	0.0007
55.5	99.50	99.52	99.54	0.50	0.48	0.46	0.001	0.0004	0.0007
57.3	99.48	99.49	99.48	0.52	0.51	0.52	0.001	0.0006	0.0007
88.2	97.73	97.70	97.92	**2.27**	**2.30**	**2.07**	0.002	0.0012	0.0035
166	98.00	97.77	96.92	**1.98**	**2.21**	**3.06**	0.013	0.0147	0.0085
176	97.92	97.77	96.17	**2.07**	**2.21**	**3.81**	0.009	0.0115	0.0075
183	97.69	98.48	98.86	**2.29**	**1.50**	**1.12**	0.009	0.0108	0.0083
190	98.23	97.94	97.80	**1.75**	**2.03**	**2.18**	0.011	0.0138	0.0111

Simulated ATMS Brightness Temperatures over Ocean Conditions

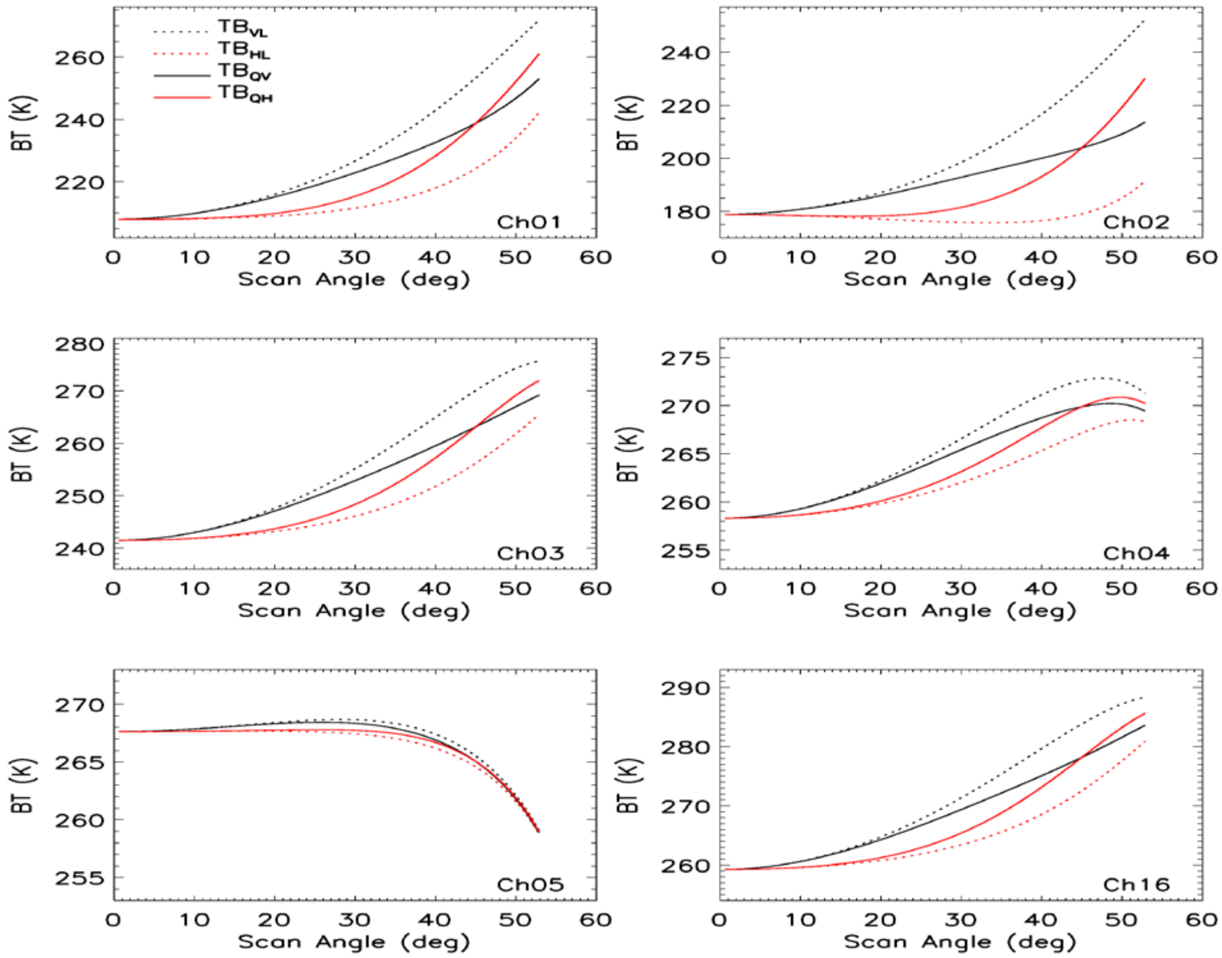

For a scan angle ranging from 15 to 45 degrees, ATMS brightness temperatures at ch1, 2, 3,4 and 16 are highly polarized over ocean conditions.

ATMS O-B Using Approach One: (Observation TDR- Simulation SDR)

For Quasi-V:

$$T_a^{Qv} - T_b^{Qv} = (\eta_{me}^{vv} - 1)T_b^{Qv} + \eta_{me}^{hv} T_b^{Qh} + \eta_{se}^{vv} E_b^{Qv} + \eta_{se}^{hv} E_b^{Qh} + \eta_{sc}^{vv} C_b^{Qv} + \eta_{sc}^{hv} C_b^{Qh} + S_a^{Qv}$$

For Quasi-H:

$$T_a^{Qh} - T_b^{Qh} = (\eta_{me}^{hh} - 1)T_b^{Qh} + \eta_{me}^{vh} T_b^{Qv} + \eta_{se}^{hh} E_b^{Qh} + \eta_{se}^{vh} E_b^{Qv} + \eta_{sc}^{hh} C_b^{Qh} + \eta_{sc}^{vh} C_b^{Qv} + S_a^{Qv}$$

For ATMS temperature sounding channels, the earth scene is un-polarized and the bias is mainly driven by the near-field side lobe effect after the far-field side-lobe effects are neglected. Fortunately, the near field side-lobe contribution is being characterized by means of its pitch-over measurements:

$$T_a^{Qh} - T_b^{Qh} \approx S_a^{Qh}$$

ATMS Pitch-Over Maneuver Data

ATMS TDR at Ch18 on February 20, 2102

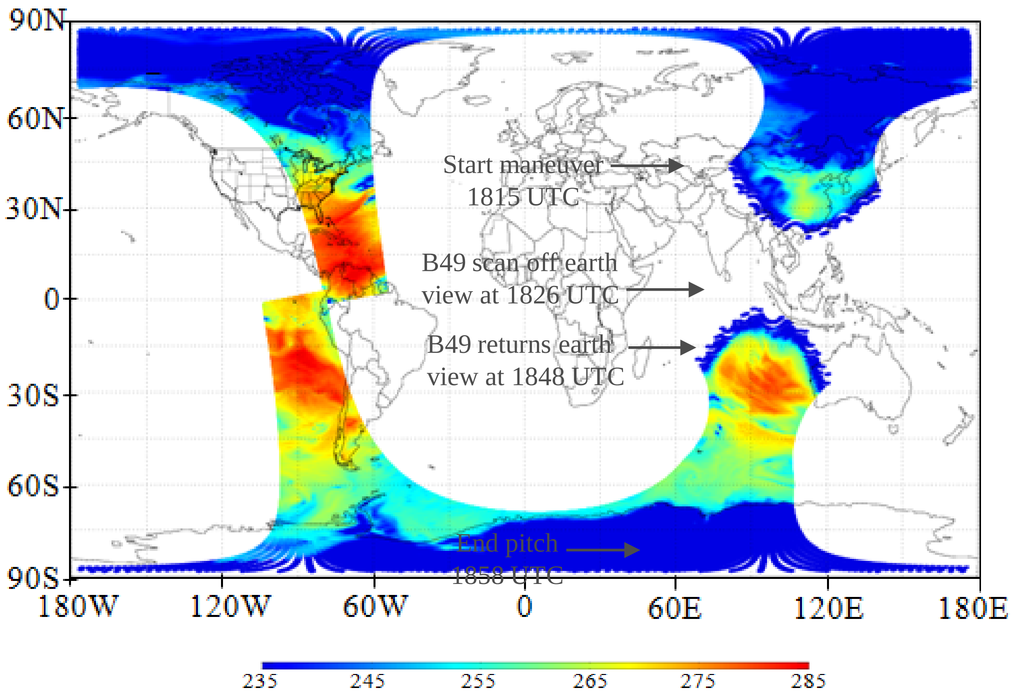

ATMS Pitch-Over TDR at Ch4

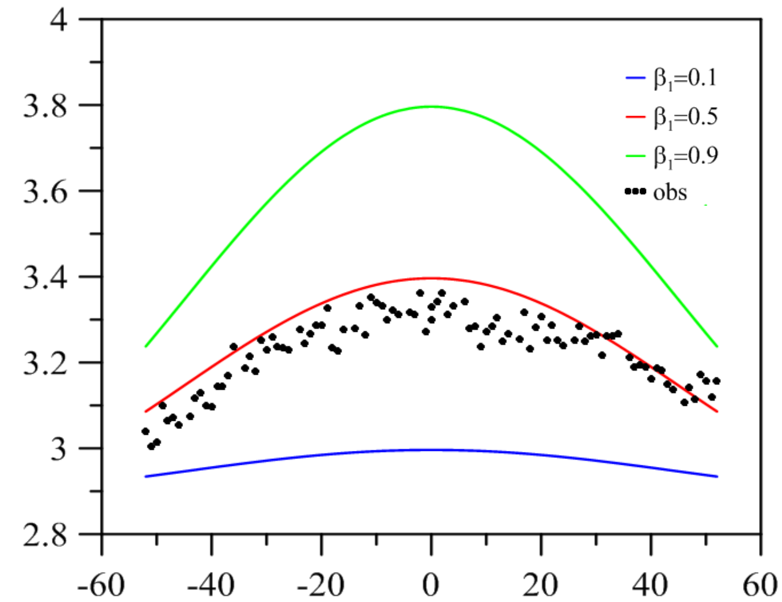

ATMS O (TDR) - B (SDR) wrt ECMWF

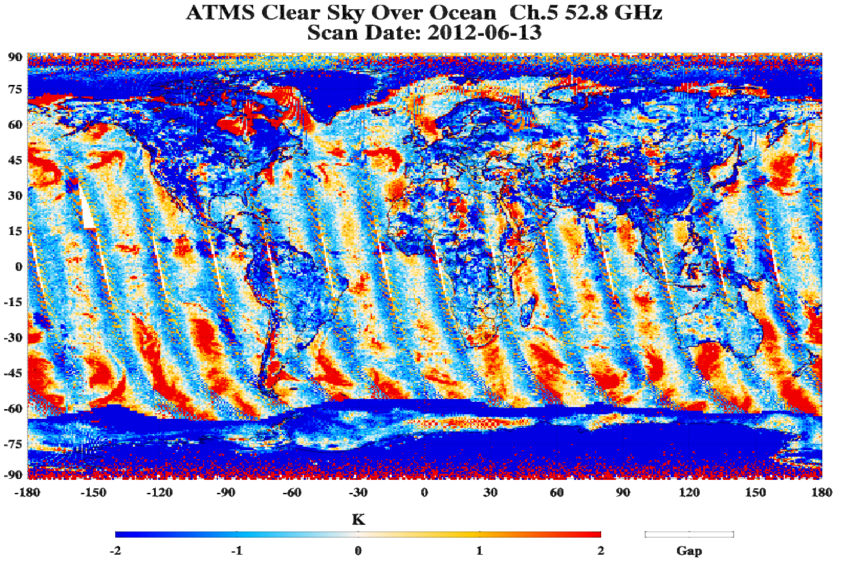

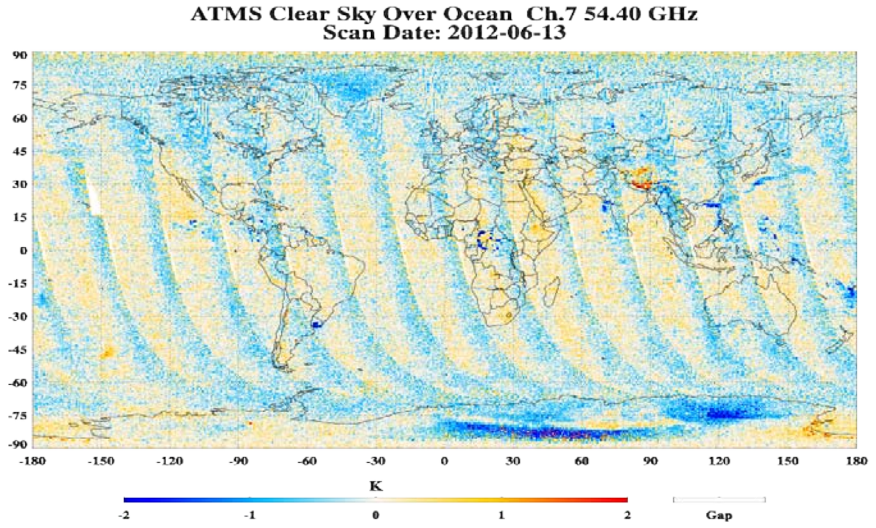

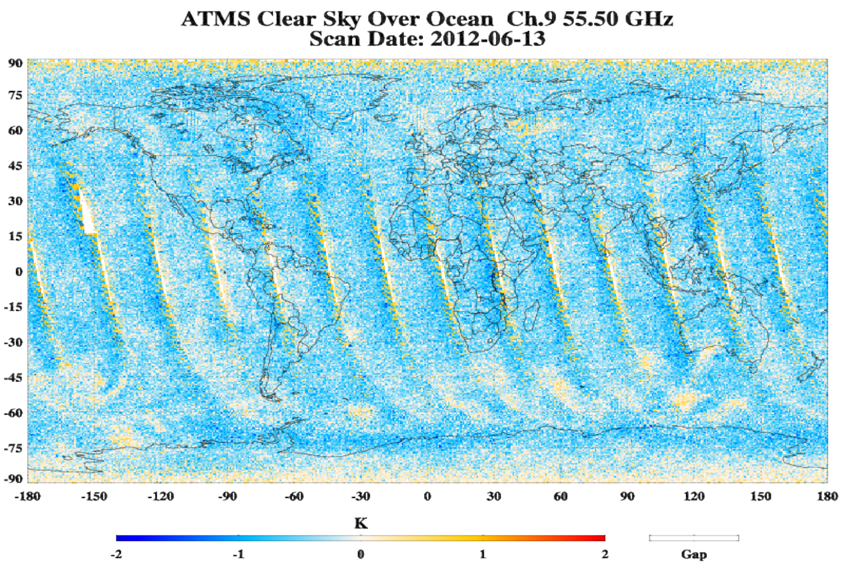

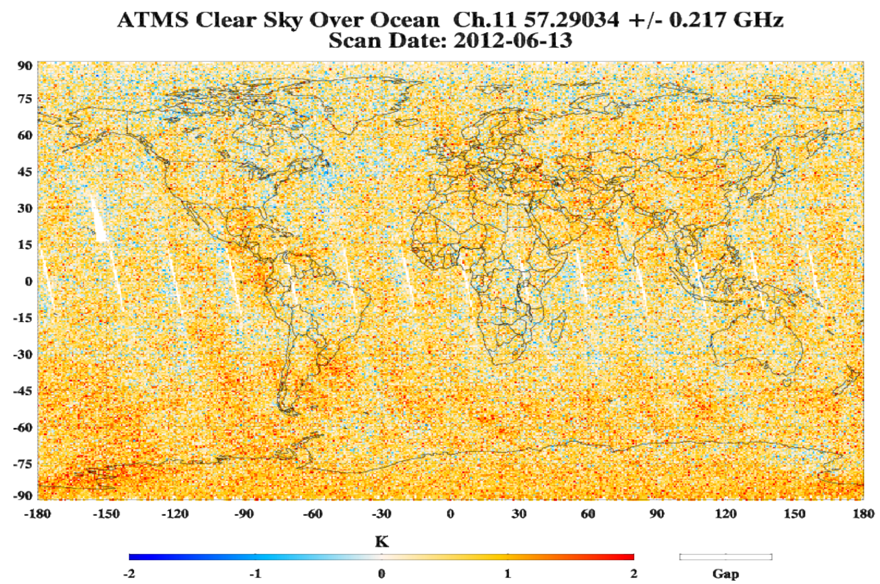

ATMS O-B Distribution for Clear Sky Conditions

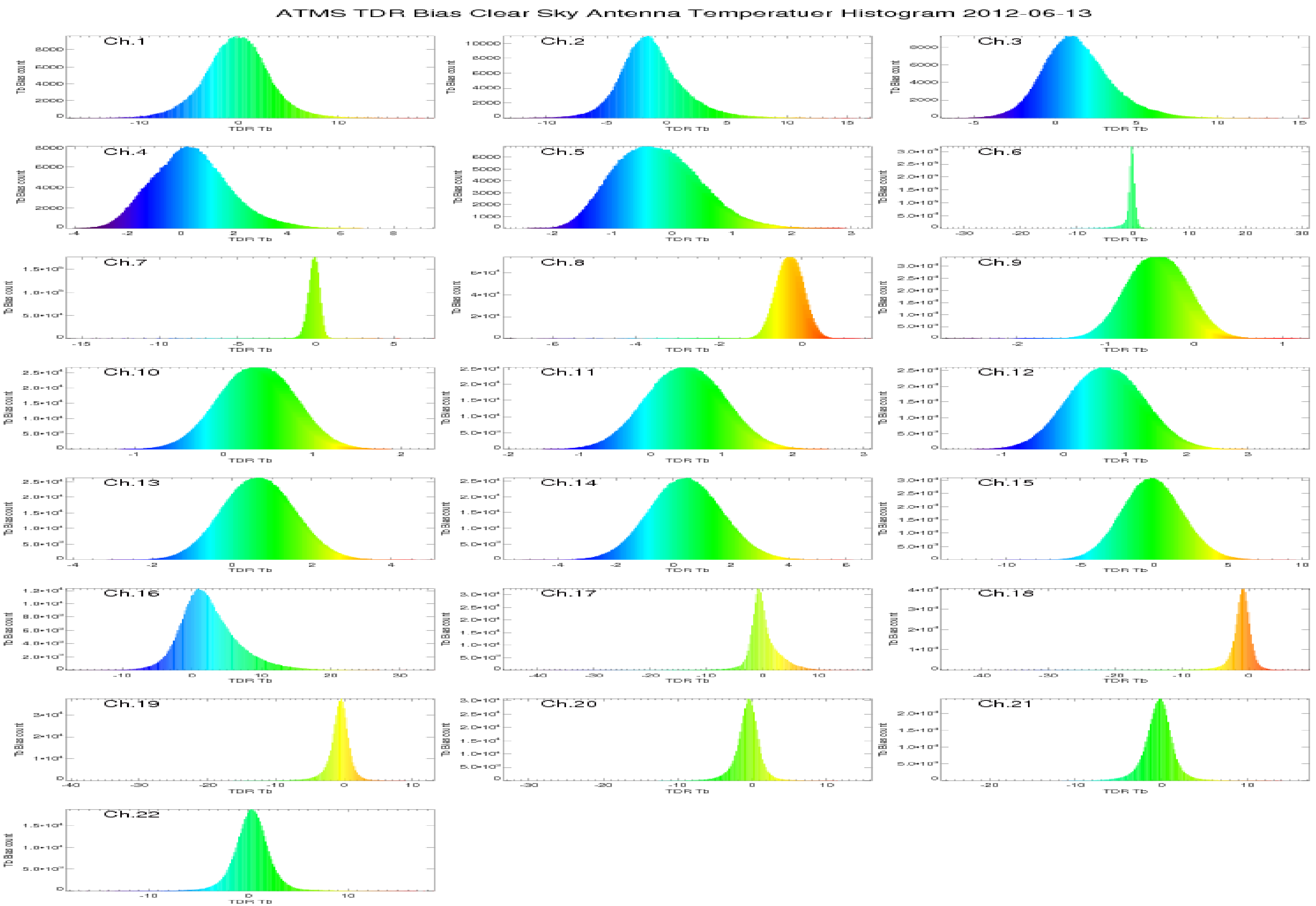

Cloud Liquid Water Algorithm

$$L = a_0 \mu [\ln(T_s - T_{b31}) - a_1 \ln(T_s - T_{b23}) - a_2]$$

μ — cosine of satellite zenith angle

T_s — surface temperature

T_{b23}, T_{b31} — brightness temperature at 23.8 and 31.4 GHz

$$a_0 = -0.5\kappa_{v23} / (\kappa_{v23}\kappa_{l31} - \kappa_{v31}\kappa_{l23}),$$

$$a_1 = \kappa_{v31} / \kappa_{v23},$$

$$a_2 = -2.0(\tau_{o31} - a_1\tau_{o23})/\mu + (1.0 - a_1)\ln(T_s) + \ln(1.0 - \varepsilon_{31}) - a_1 \ln(1.0 - \varepsilon_{23})$$

κ_v — water vapor absorption coefficients

κ_l — cloud liquid water mass absorption coefficients

τ_o — optical thickness

Weng, F., L. Zhao, R. R. Ferraro, G. Poe, X. Li, and N. C. Grody, Advanced microwave sounding unit cloud and precipitation algorithms, Radio Sci., 38(4), 8086, 2003.

ATMS Brightness Temperature at CH 2

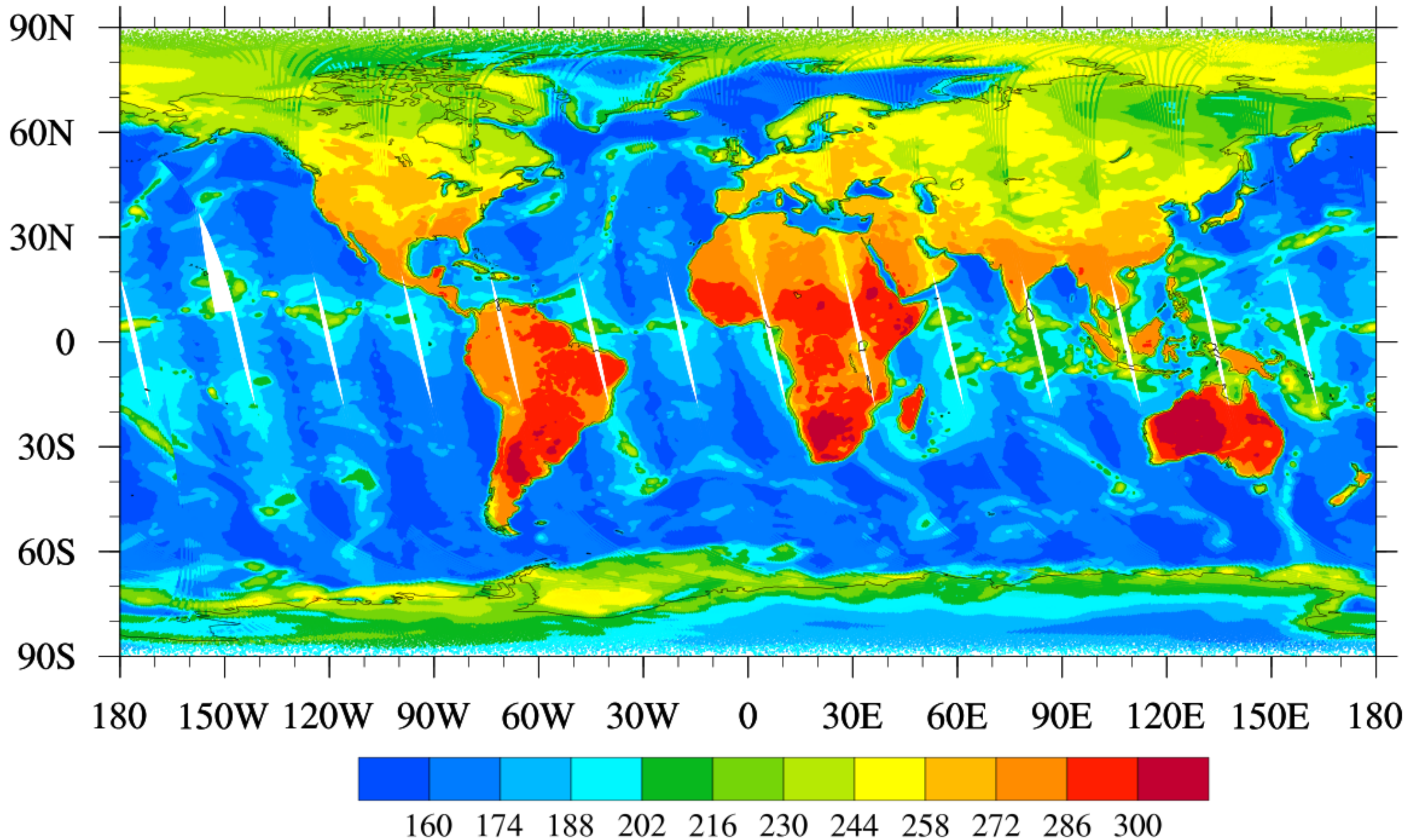

December 20, 2011

ATMS Cloud Liquid Water

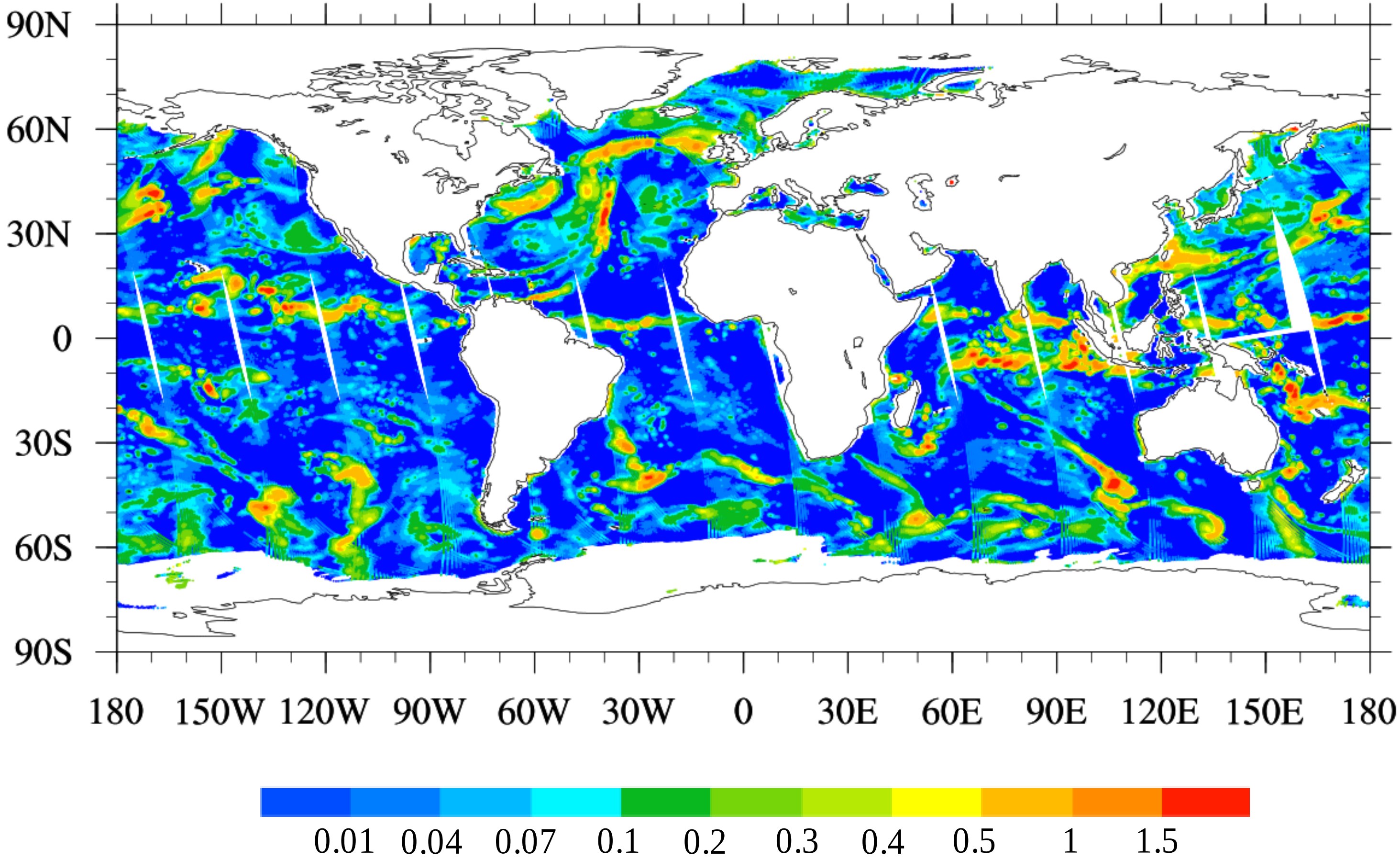

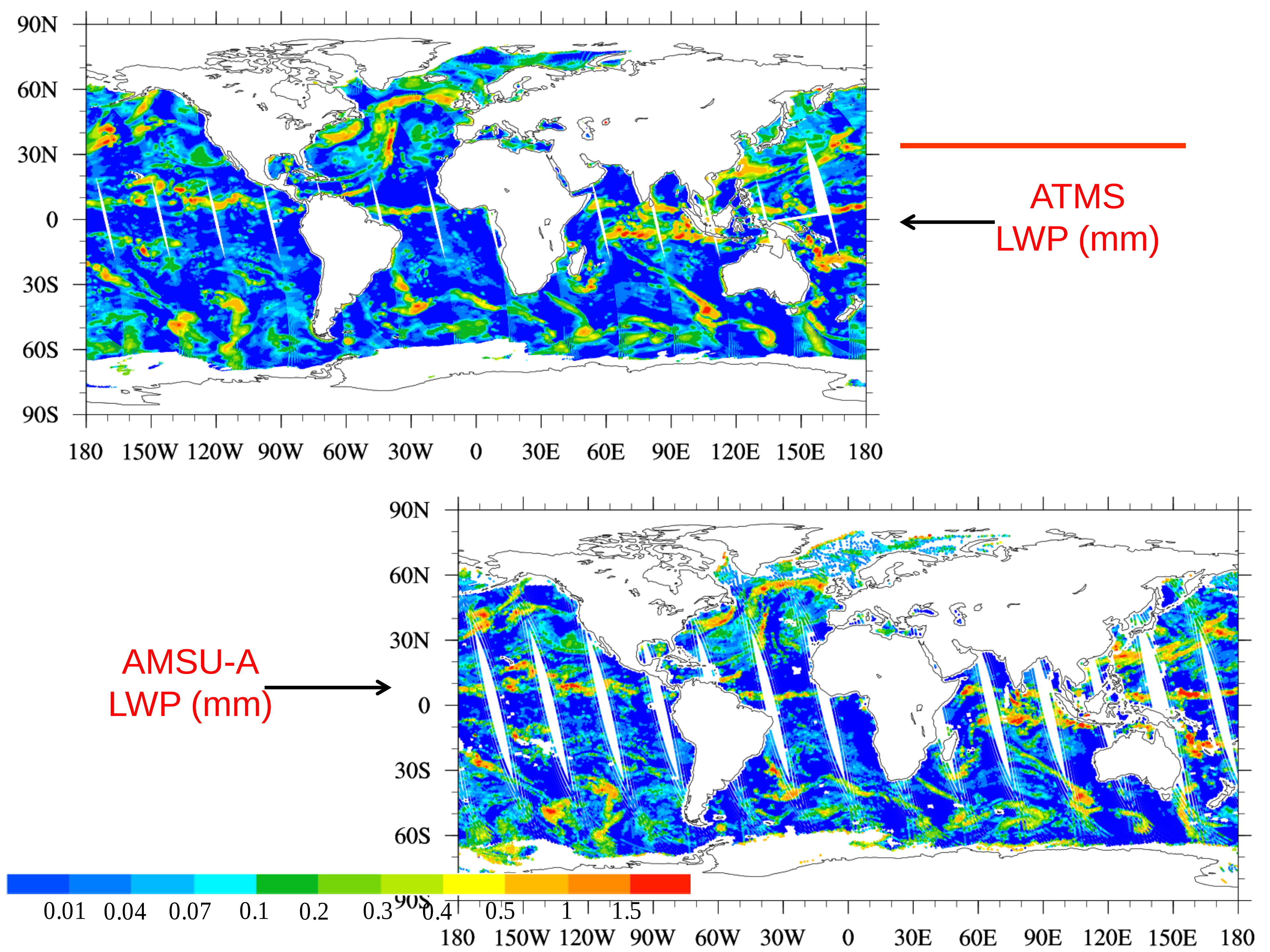
ATMS
LWP (mm)
AMSU-A
LWP (mm)
90N
60N
30N
0
30S
60S
90S
180
150W
120W
90W
60W
30W
0
30E
60E
90E
120E
150E
180
0.01
0.04
0.07
0.1
0.2
0.3
0.4
0.5
1
1.5

Scene-Temperature Dependence of Biases

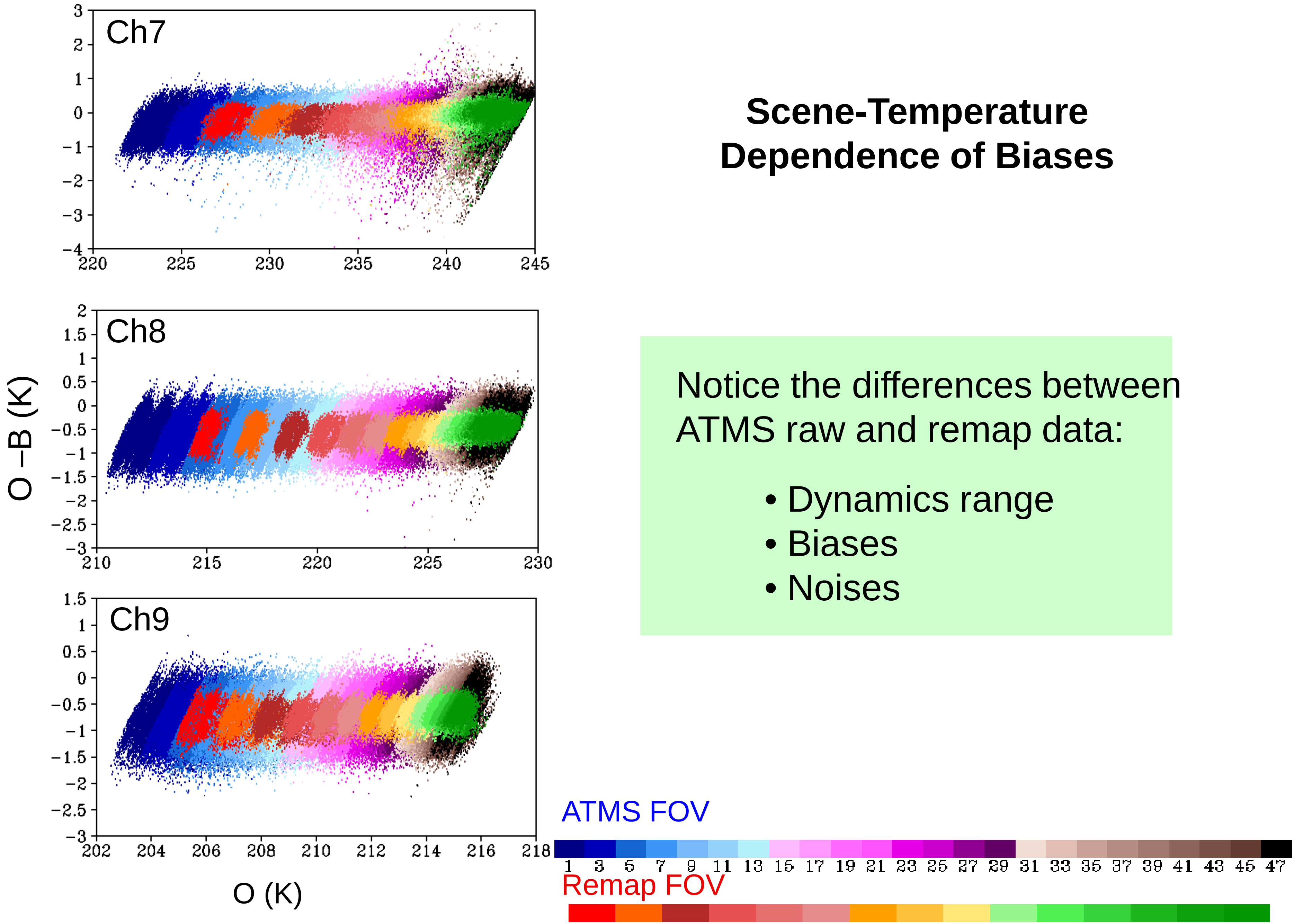

Notice the differences between ATMS raw and remap data:

- Dynamics range
- Biases
- Noises

Global Biases and Standard Deviations

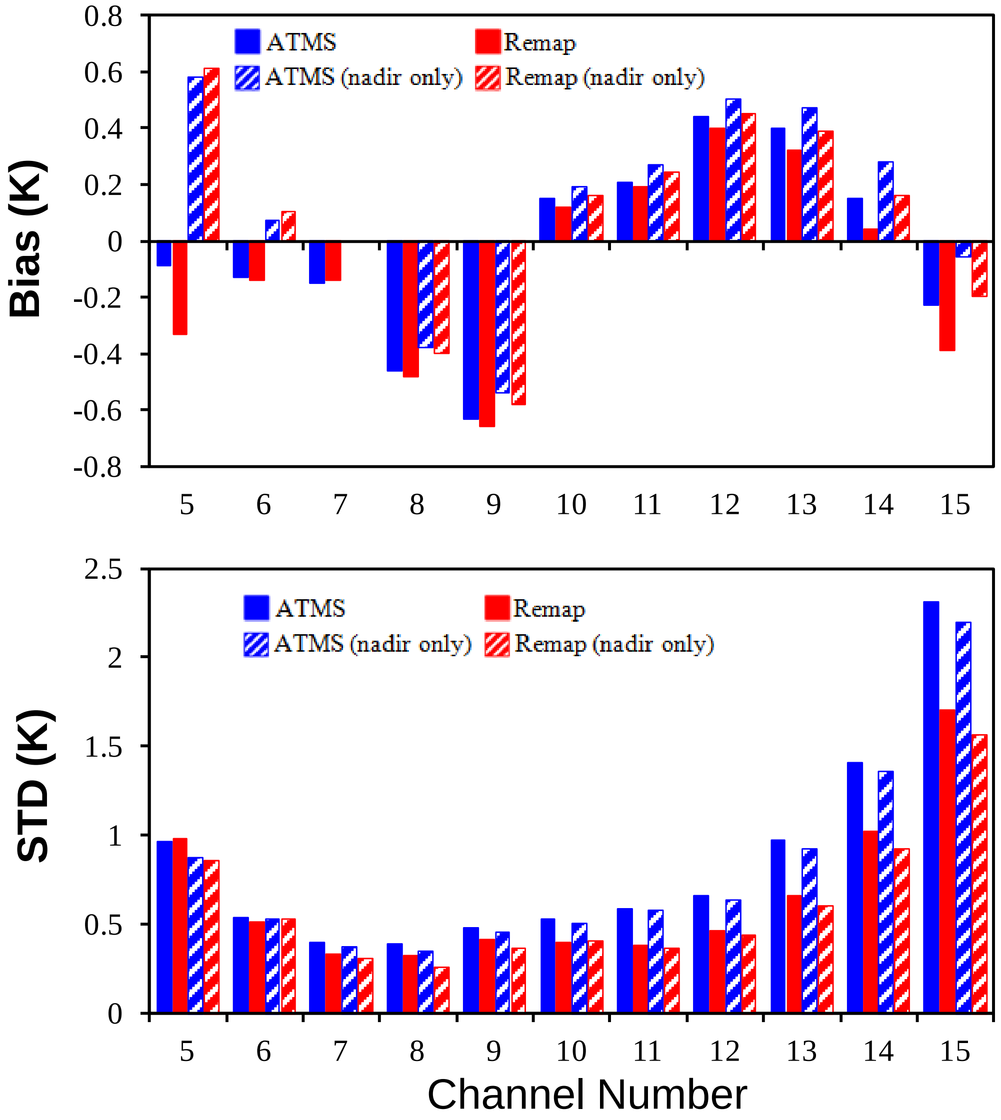

Within 60S-60N, clear-sky, ocean only, 20-27 December 2011

Scan Dependence of Biases

Nadir bias subtracted

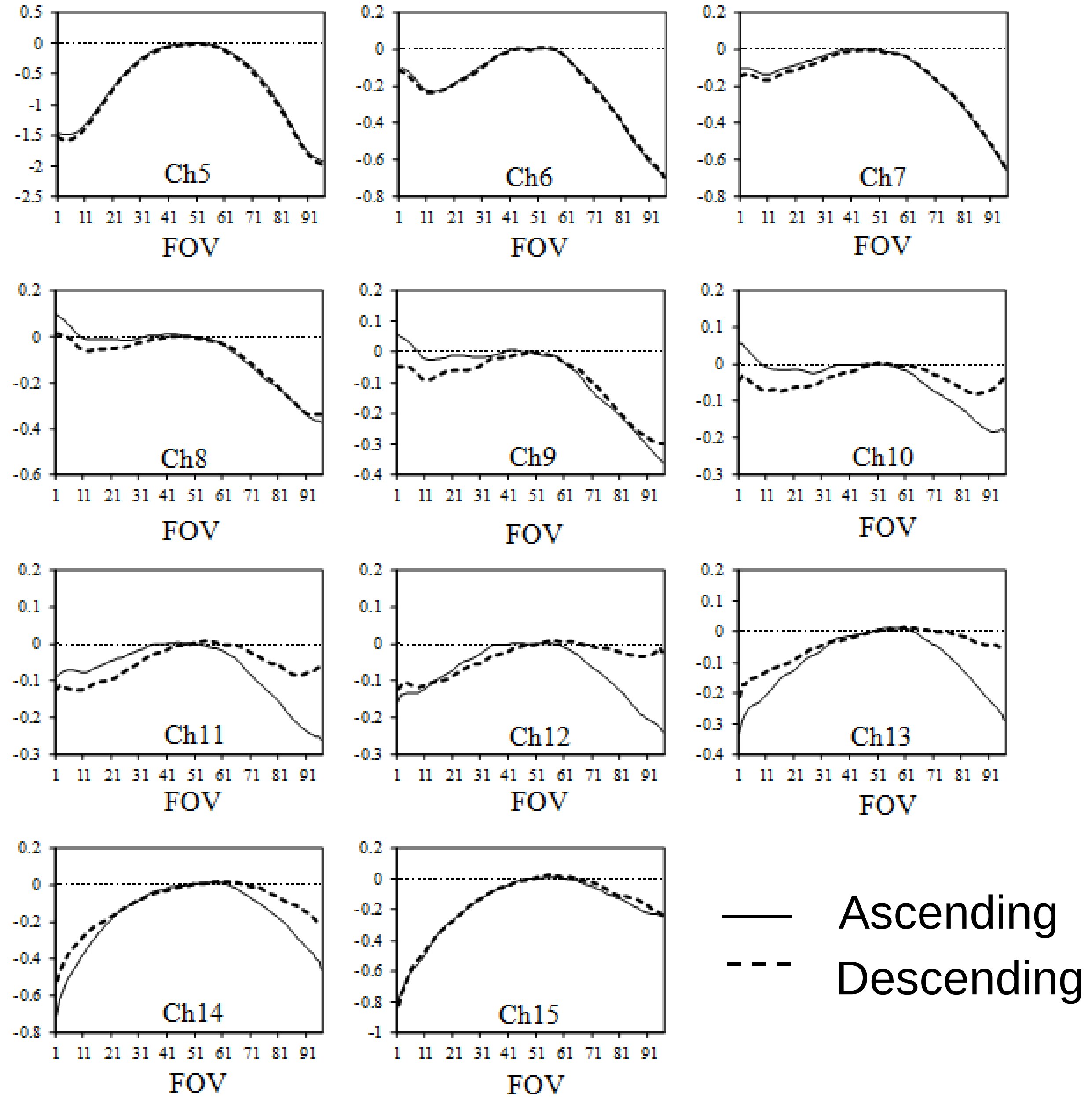

Effects of NWP Model Top Heights on O-B

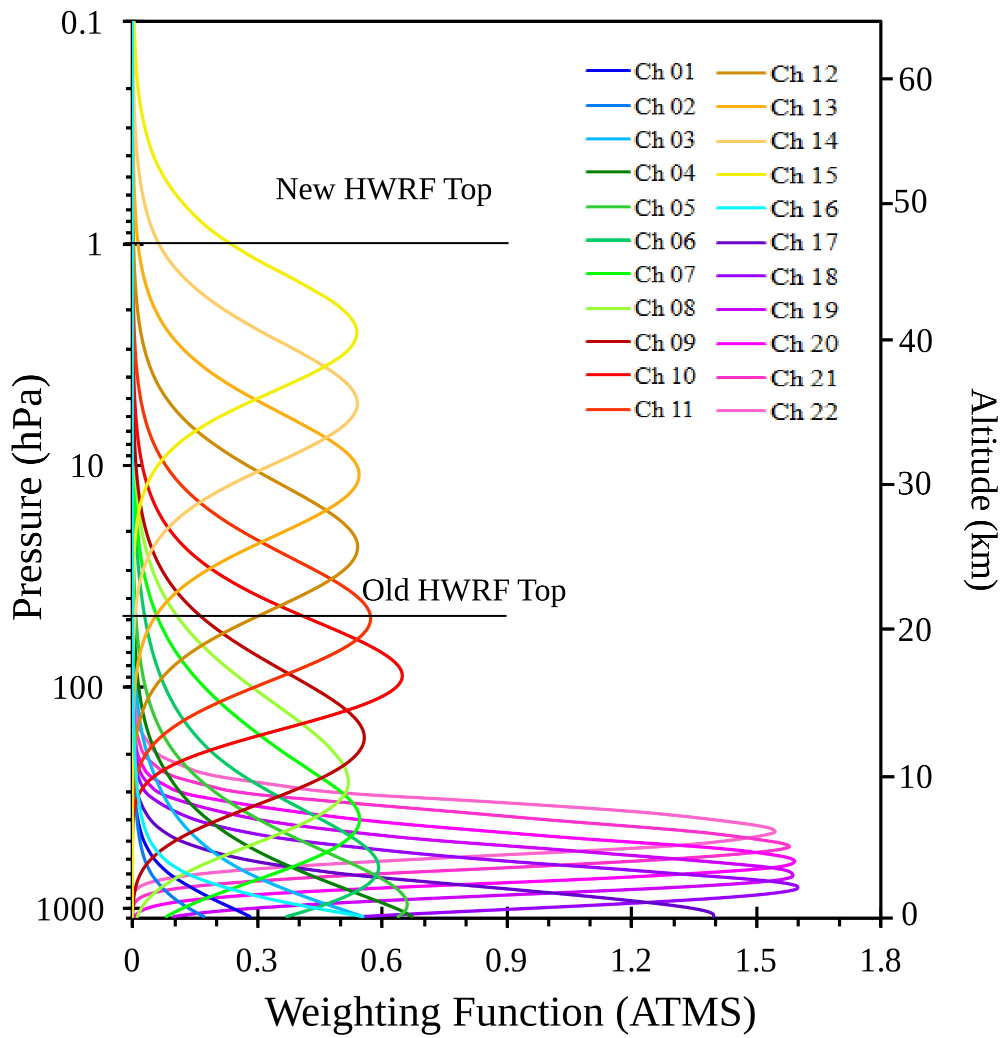

If an NWP model top (such as HWRF) is run at 50 hPa, many of satellite upper level sounding channels can not be assimilated due to large O-B

ATMS Simulated Tb at Ch14 and Temperature at 4.9 hPa

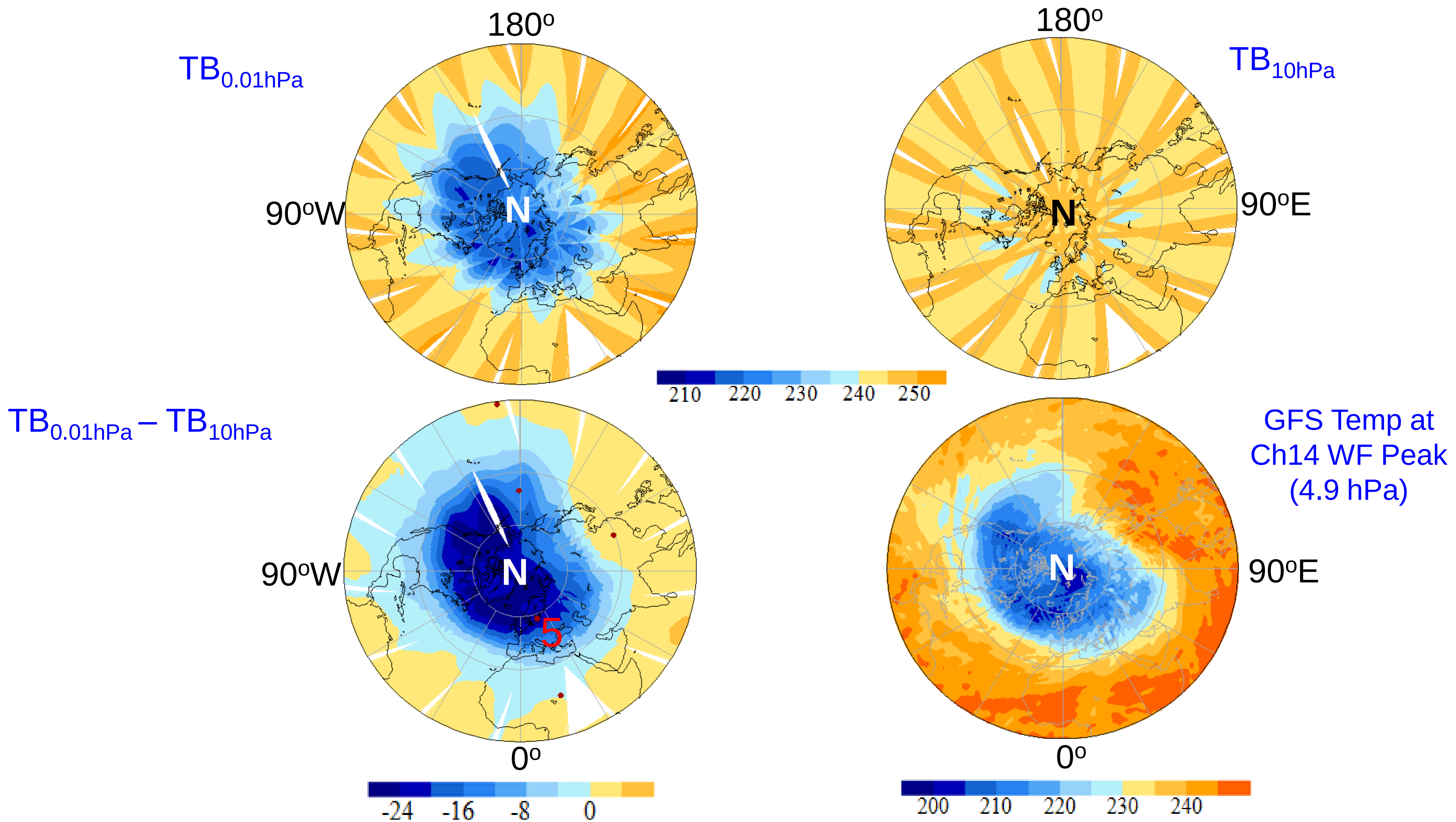

0000-1200 UTC on December 20, 2011

Comparison of GFS 64-level and 26-level Data

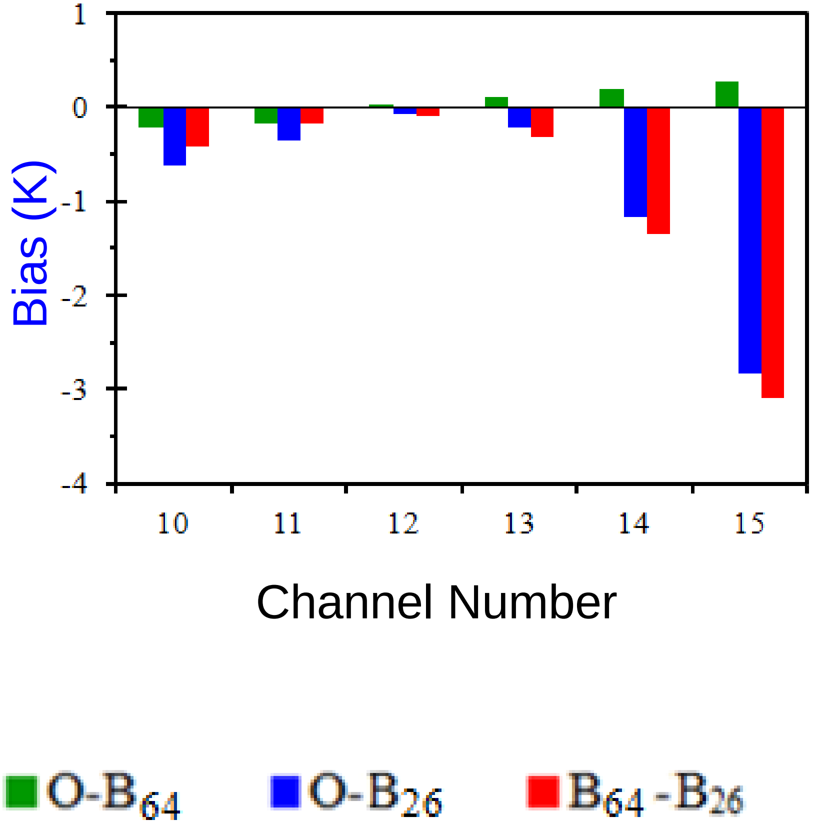

Model top level pressure

GFS 64: 0.01hPa

GFS 26: 10hPa

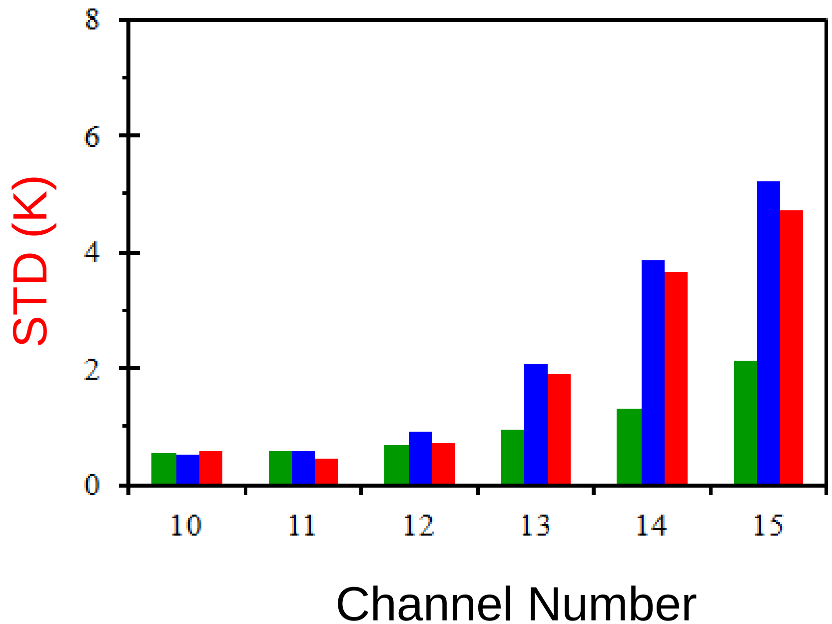

20-27 December 2011

Uses of GPSRO Data for ATMS Bias Characterization

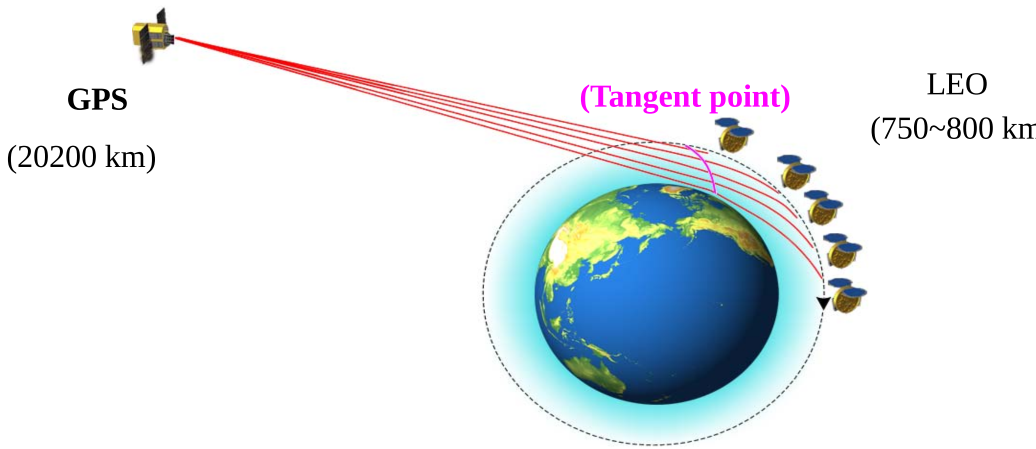

1. High vertical resolution
2. No contamination from clouds
3. No system calibration required
4. High accuracy and precision:

The global mean differences between COSMIC and high-quality reanalyses is ~0.65K between 8 and 30km (Kishore et al. 2008)

The precision of COSMIC GPS RO soundings is ~0.05K in the upper troposphere and lower stratosphere (Anthes et al. 2008)

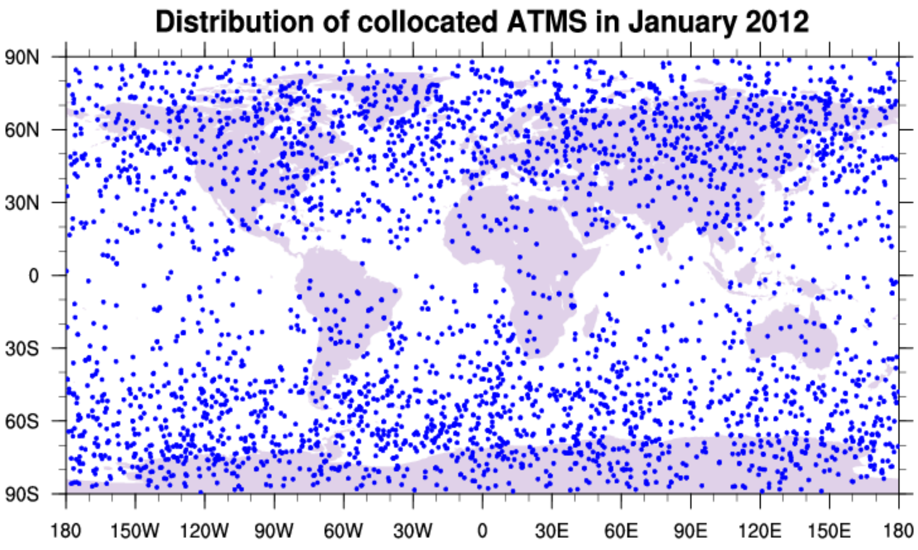

- **Time period of data :** January, 2012
- **Collocation of ATMS and COSMIC data:** Time difference < 0.5 hour, Spatial distance < 30 km , GPS geolocation at 10km altitude is used for spatial collocation)

ATMS Bias Distribution Using GPSRO

Ch08

O **O-B**

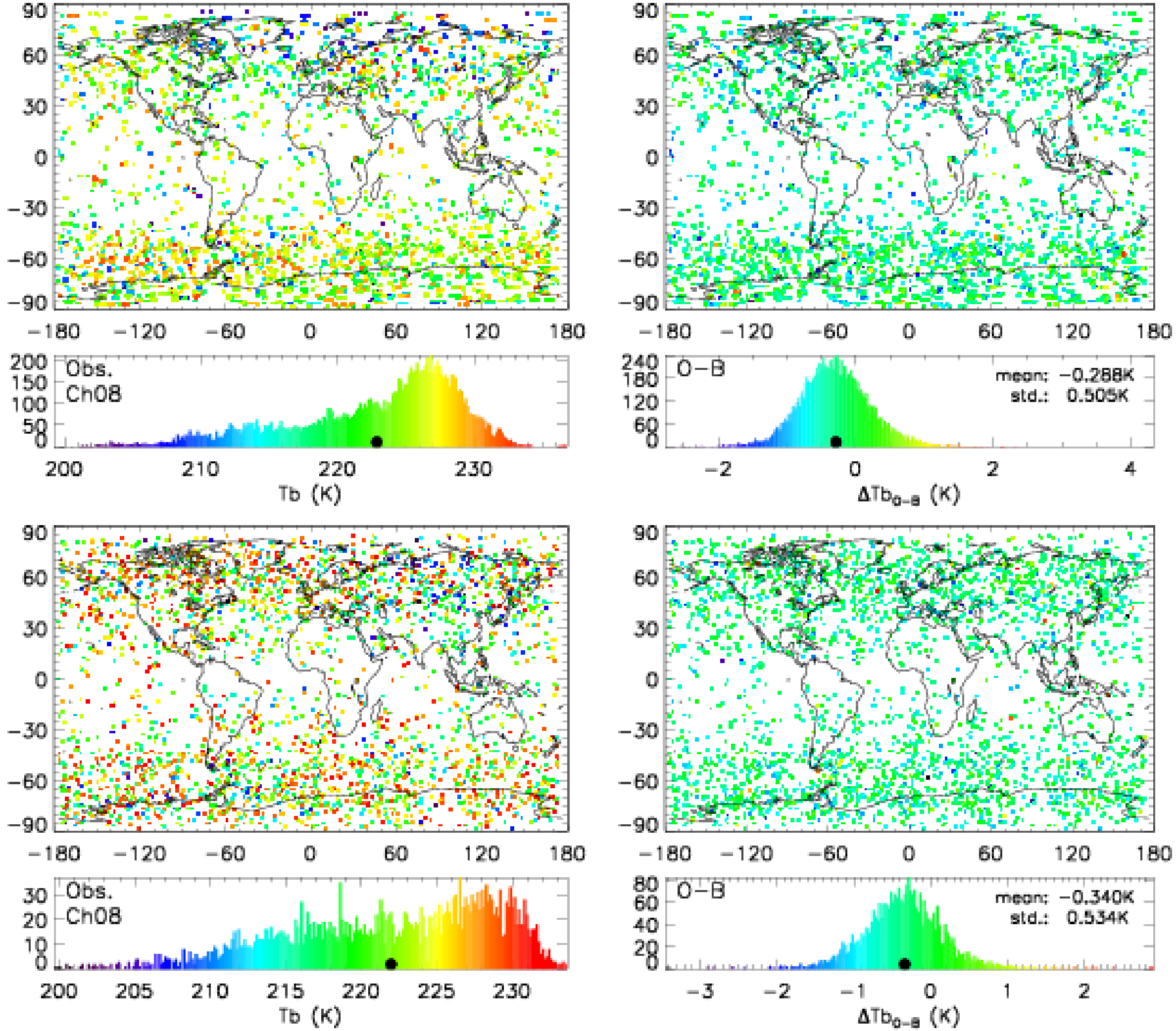

December, 2011

January, 2012

Post-Launch ATMS Calibration Accuracy Using COSMIC Data

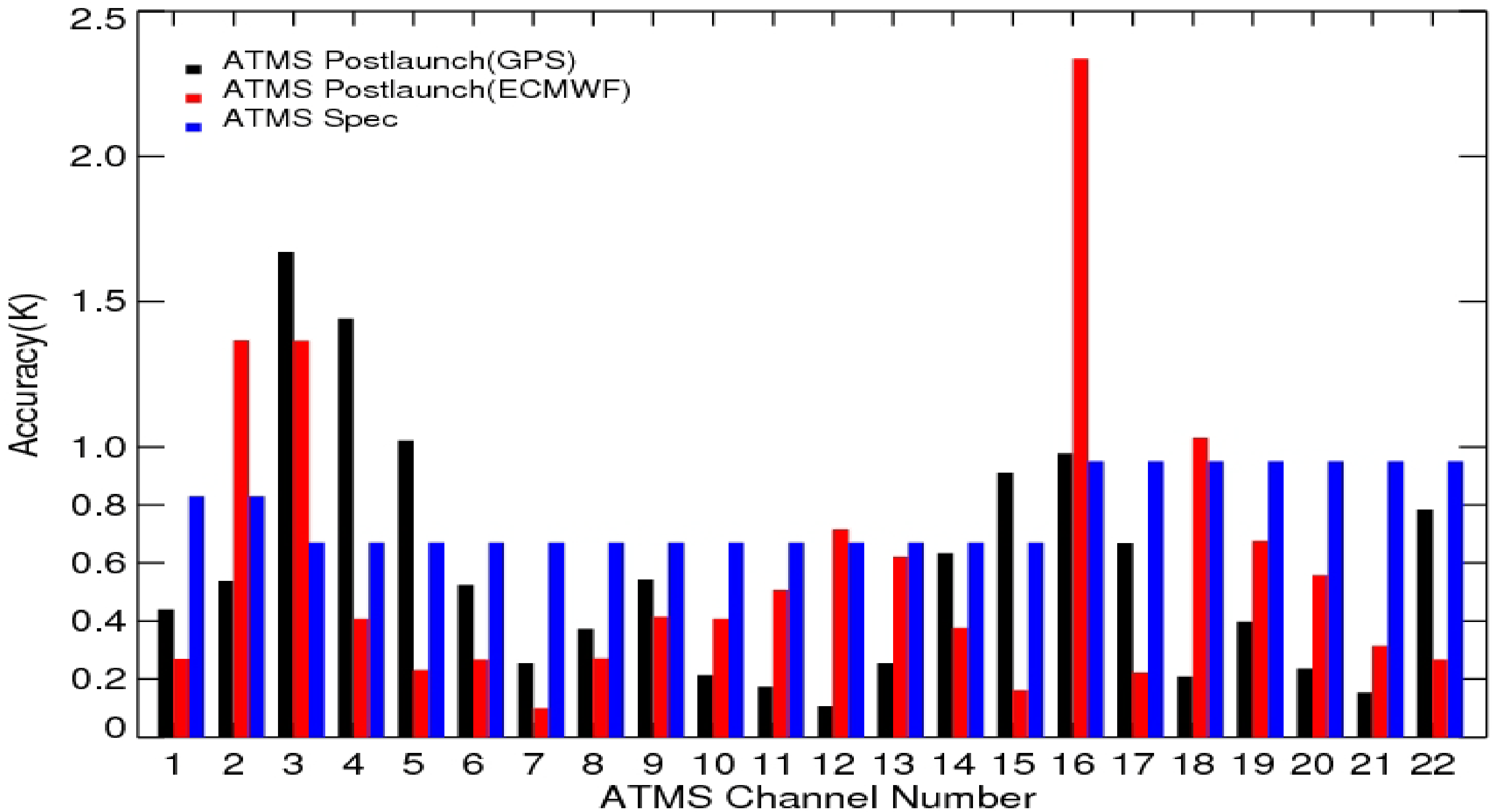

On-orbit ATMS calibration accuracy is quantified using GPSRO data as input to LBLRT model and the results are better than specification for most of sounding channels

Suomi NPP ATMS Resolves Warm Core Strcuture of Tropical Cyclones

Giovanna at Feb 13 2012 0630Z
MODIS Visible Channel

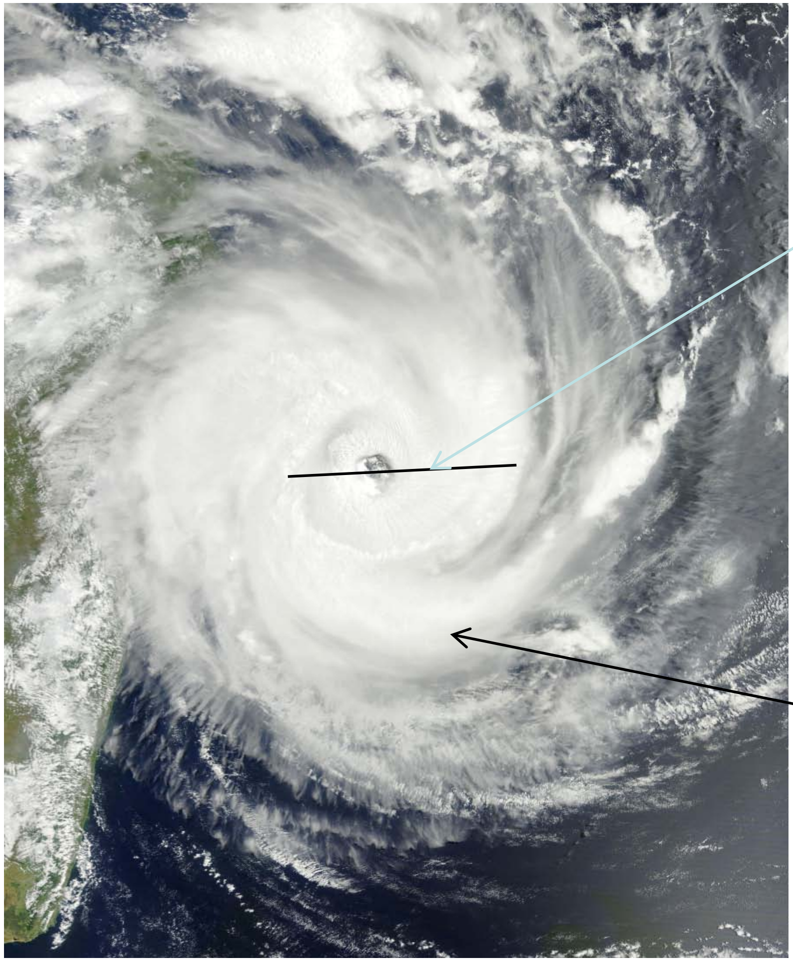

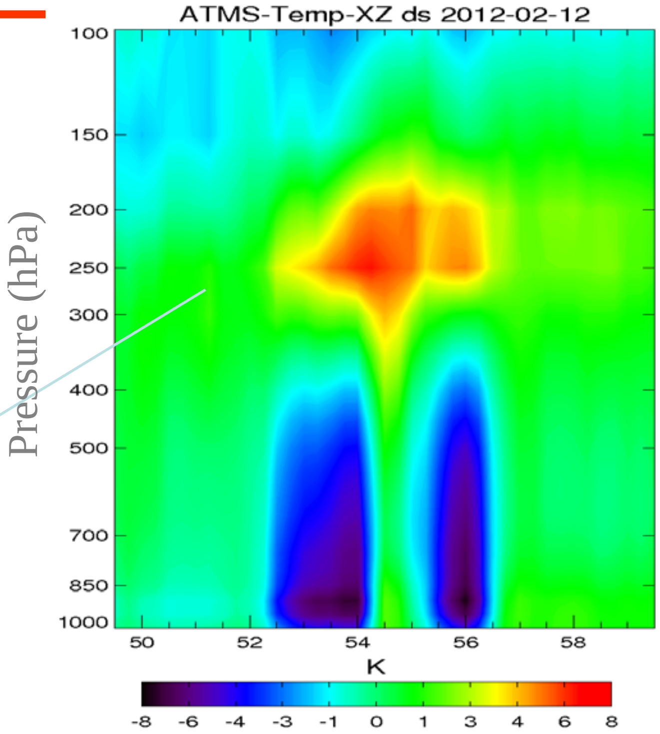

A warm core of 8K ore more at 250 hPa from ATMS indicated a category 4 to 5 hurricane intensity

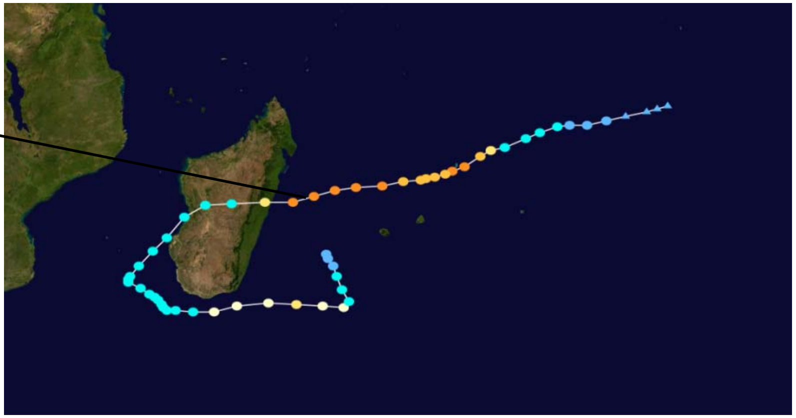

SSMIS Channel Characteristics

SSMIS Sensor Characteristics

Channel	Center Freq.(GHz)	Passband (MHz)	Freq. Stab.(MHz)	Pol	NEDT (Max)(K)	S In
1	50.3	400	10	H	0.4	
2	52.8	400	10	H	0.4	
3	53.596	400	10	H	0.4	
4	54.4	400	10	H	0.4	
5	55.5	400	10	H	0.4	
6	57.29	350	10	*	0.5	
7	59.4	250	10	*	0.6	
8	150	1500	200	H	0.88	
9	183.31+/-6.6	1500	200	H	1.2	
10	183.31+/-3	1000	200	H	1.0	
11	183.31+/-1	500	200	H	1.25	
12	19.35	400	75	H	0.7	
13	19.35	400	75	V	0.7	
14	22.235	400	75	V	0.7	
15	37	1500	75	H	0.5	
16	37	1500	75	V	0.5	
17	91.655	3000	100	V	0.9	
18	91.655	3000	100	H	0.9	
19	63.283248 +/-0.285271	3	0.08	V + H	2.4	
20	60.792668 +/-0.357892	3	0.08	V + H	2.4	
21	60.792668 +/-0.357892 +/-0.002	6	0.08	V + H	1.8	
22	60.792668 +/-0.357892 +/-0.006	12	0.12	V + H	1.0	
23	60.792668 +/-0.357892 +/-0.016	32	0.34	V + H	0.6	
24	60.792668 +/-0.357892 +/-0.050	120	0.84	V + H	0.7	

Notes:

1. The sampling interval refers to the along scan direction and is based on nominal spacec
2. The radiometer integration time is 4.20msec for a single 12.5km sample interval.
3. * = These channels are not polarization dependent.

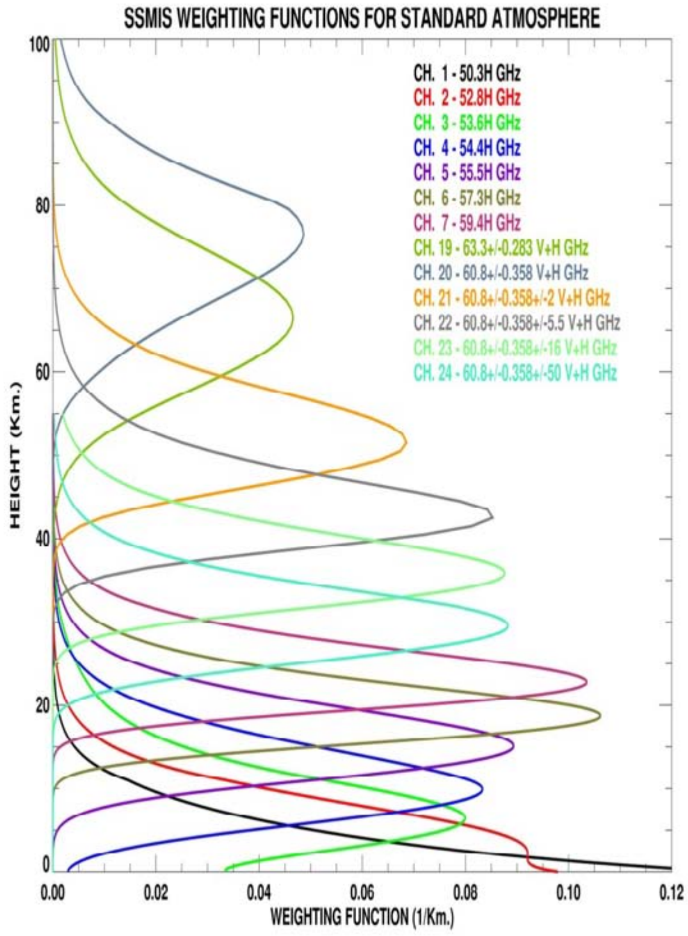

SSMIS Scanning Characteristics

- 24 Channels (19-183 GHz)
- Conical Scan Geometry
- Mesospheric Sounding
- Improved Sounding HCS
- Swath Width 1700 km
- Scan Rate 31.6 rpm
- Calibration Accuracy
  - Better than 1K
  - Warm and Cold Targets each Scan

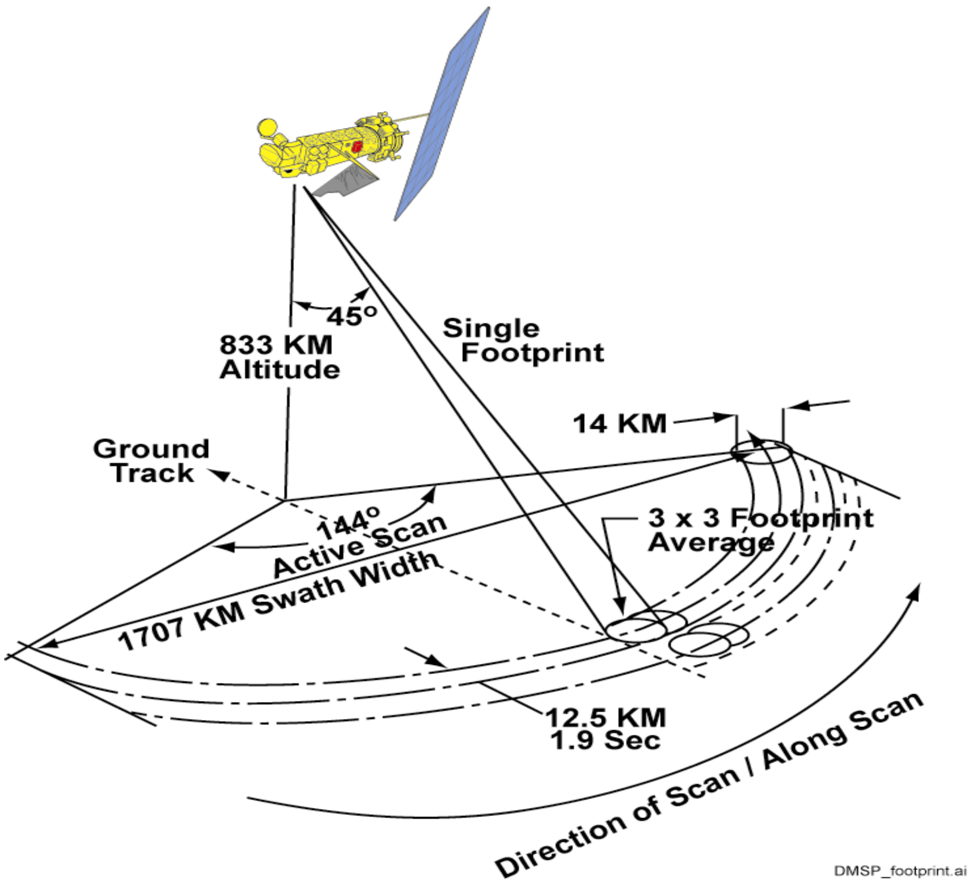

Antenna/Sensor Brightness Temperature for Conical Scanning Instrument

SDR

TDR

$$T_a^v = \eta_{me}^{vv} T_b^v + \eta_{me}^{hv} T_b^h + \eta_{se}^{vv} E_b^v + \eta_{se}^{hv} E_b^h + \eta_{sc}^{vv} C_b^v + \eta_{sc}^{hv} C_b^h + S_b^v$$

SDR

$$T_a^h = \eta_{me}^{hh} T_b^h + \eta_{me}^{vh} T_b^v + \eta_{se}^{hh} E_b^h + \eta_{se}^{vh} E_b^v + \eta_{sc}^{hh} C_b^h + \eta_{sc}^{vh} C_b^v + S_b^h$$

For a microwave conical scanning radiometer, the cross-polarization term is measured at imaging channels. Thus, sensor brightness temperatures can be derived from antenna brightness temperature measurements

Anomalies in SSMIS Antenna System

- Main-reflector conically scans the earth scene
- Sub-reflector views cold space to provide one of two-point calibration measurements
- Warm loads are directly viewed by feedhorn to provide other measurements in two-point calibration system
- The SSMIS main reflector emits radiation from its coating material
  - SiOx VDA (coated vapor-deposited aluminum)
  - SiOx and Al VDA Mixture
  - *Graphite Epoxy*
- Warm load calibration is contaminated by solar and stray lights
  - Reflection Off of the Canister Top into Warm Load
  - Direct Illumination of the Warm Load Tines
- Space view is also occasionally contaminated

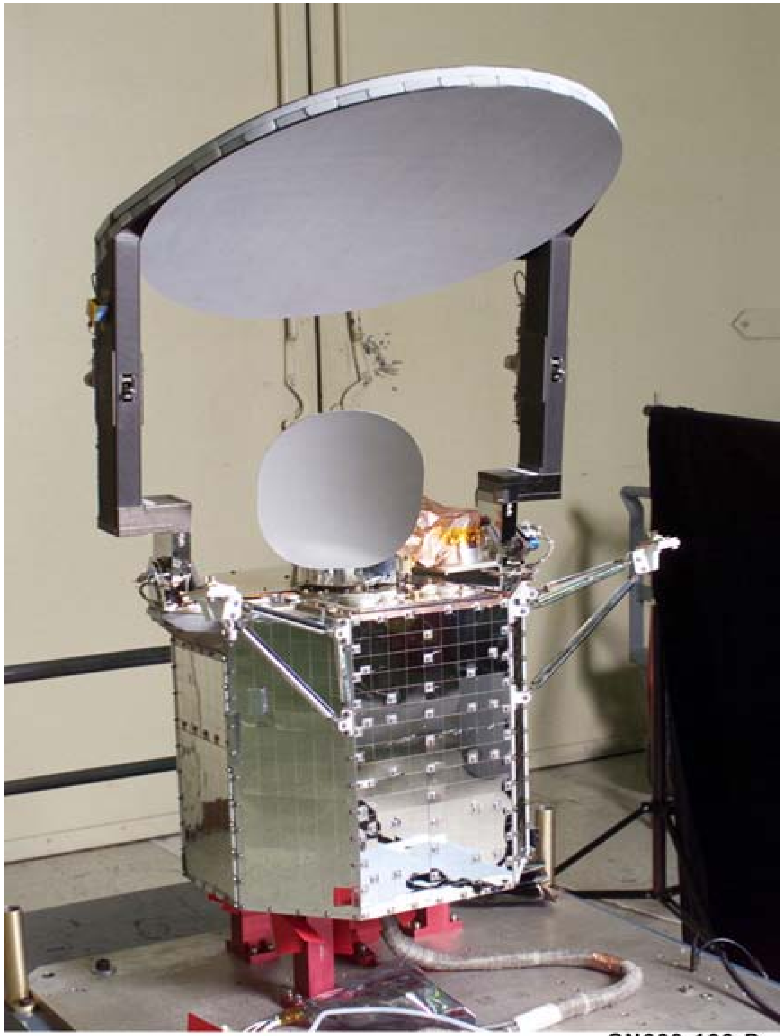
CN600-136-D

Antenna/Sensor Brightness Temperature with an Emitting Antenna

$$\begin{cases} T_a^v = (1-\varepsilon_r^v)[\eta_{me}^{vv} T_b^v + \eta_{me}^{hv} T_b^h] + \varepsilon_r^v T_r \\ T_a^h = (1-\varepsilon_r^h)[\eta_{me}^{hh} T_b^h + \eta_{me}^{vh} T_b^v] + \varepsilon_r^h T_r \end{cases}$$

Or

$$\begin{cases} T_a^v = \gamma_{me}^{vv} T_b^v + \gamma_{me}^{hv} T_b^h + \varepsilon_r^v T_r \\ T_a^h = \gamma_{me}^{hh} T_b^h + \gamma_{me}^{vh} T_b^v + \varepsilon_r^h T_r \end{cases}$$

Where $\gamma_{me}^{pq} = (1-\varepsilon_r^p)\eta_{me}^{pq}$

T_r is the antenna physical temperature

SSMIS Sounding Channel O-B (Observation TDR - Simulation SDR)

$$T_a^h - T_b^h = (\eta_{me}^{hh} + \eta_{me}^{vh} - 1 - \varepsilon_r^h \eta_{me}^{hh} - \varepsilon_r^v \eta_{me}^{vh}) T_b^h + \varepsilon_r^h T_r$$

$$T_a^h - T_b^h \approx \varepsilon_r^h (T_r - \eta_{me}^{hh} T_b^h)$$

For the SSMIS temperature sounding channels, the bias is mainly driven by the difference between the antenna reflector temperature and the earth scene brightness temperature when the side-lobe effects from near- and far- fields are negligible. If $T_r - \eta_{me}^{hh} T_b^h \approx 100\mathrm{K}$ *and an emissivity of 0.02, the bias can be on an order of 2.0K*

SSMIS Arm/Rim Temperature

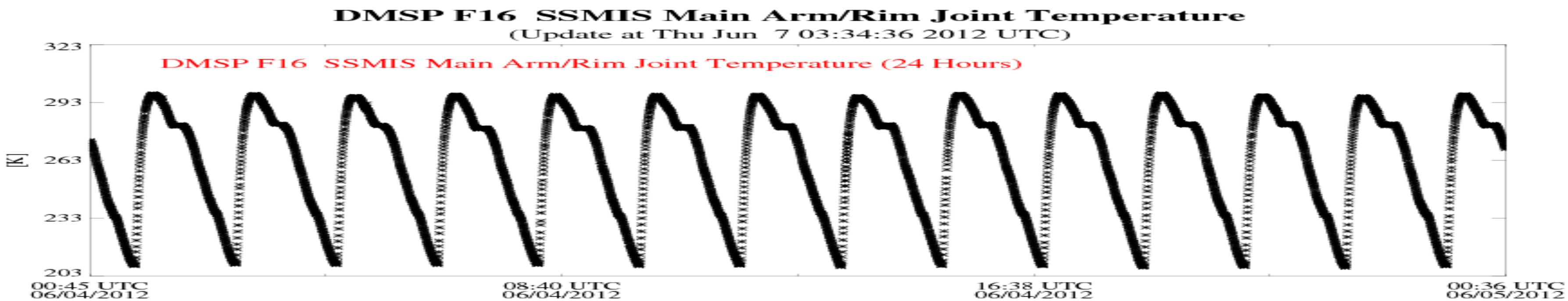

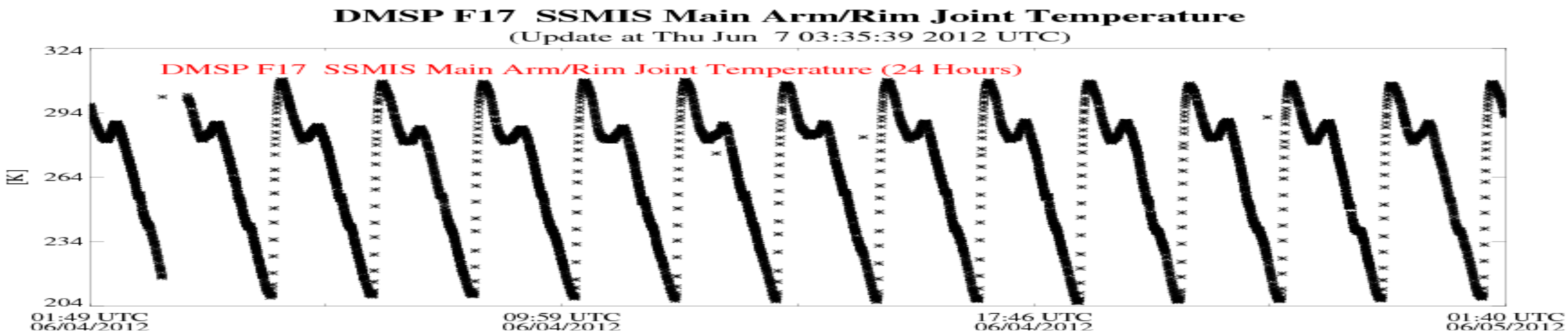

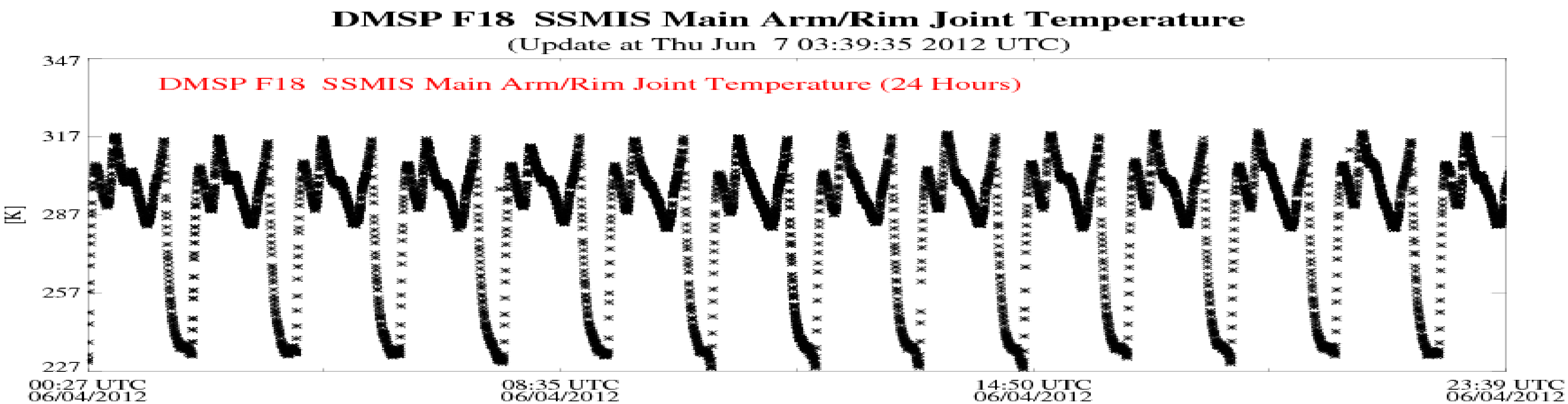

SSMIS O-B at ch3 (53.59 GHz) February 15, 2012

AS **DS**

F16

F17

F18

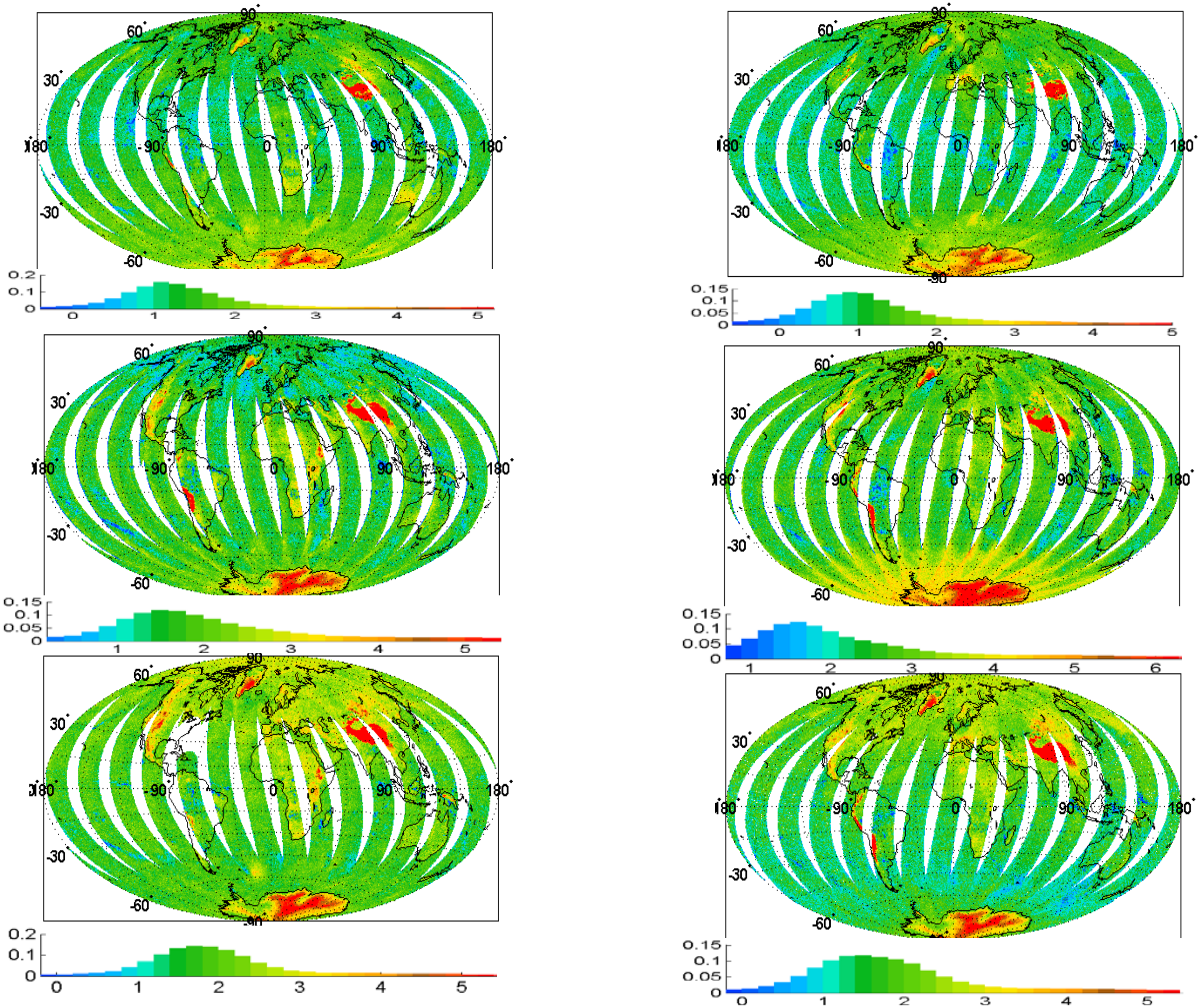

SSMIS O-B at ch5 (55.5 GHz) February 15, 2012

AS DS

F16

F17

F18

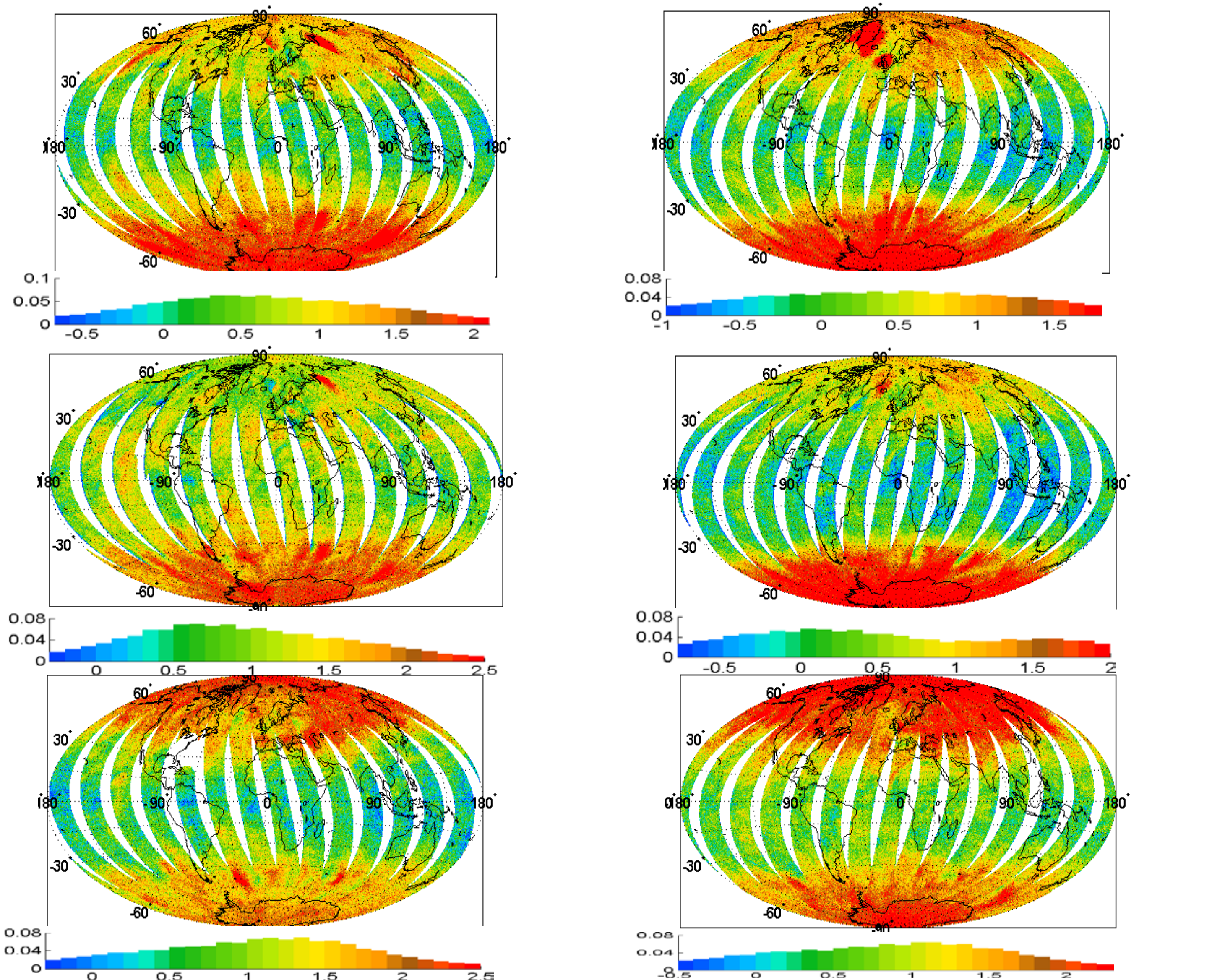

SSMIS PRT/Count

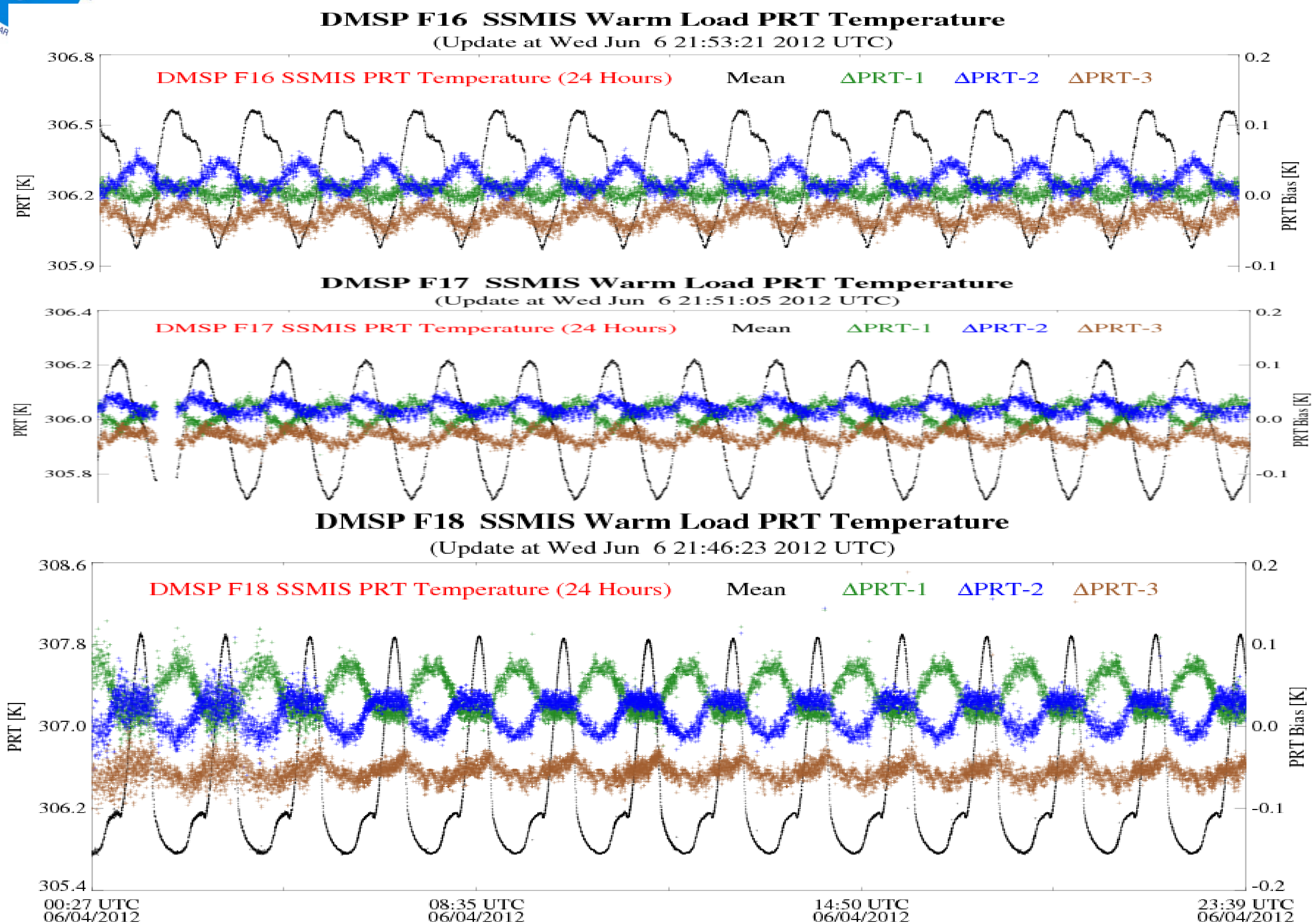

SSMIS Preprocessing and Calibration Algorithms

- NRL/UK MetOffice SSMIS Unified Pre-processor (UPP data) (Bell et al. 2008)
  - Correction of antenna emission for LAS
  - Correction of warm load anomaly
  - Linear mapping of SSMIS imager to its predecessor (SSM/I)
  - Doppler shift correction for UAS
  - Spatial averaging to reduce to the sub-Kelvin levels

- NOAA/NESDIS SSMIS Pre-processor (NESDIS Data) (Yan and Weng 2009)
  - Correction of antenna emission for LAS
  - Correction of warm load anomaly
  - UAS bias removal using SABER (Sounding of the Atmosphere using Broadband Emission Radiometry) measurements simulated as truth
  - Spatial filter for noise reduction
  - Linear mapping of SSMIS imager to its predecessor (SSM/I) using the F15 and F16 Simultaneous Conical Overpass observations
  - Inter-sensor calibration for SSMIS imager non-linearity (for climate reprocessing)

F16 SSMIS O-B (Ch5)

Before anomaly correction

After anomaly correction

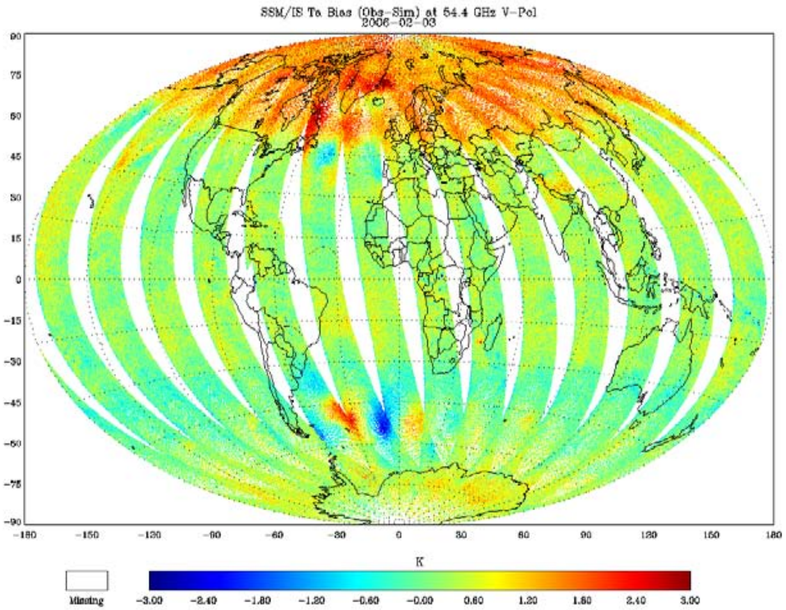

Uncorrected Ch 4 OB-BK (GDAS CRTM)

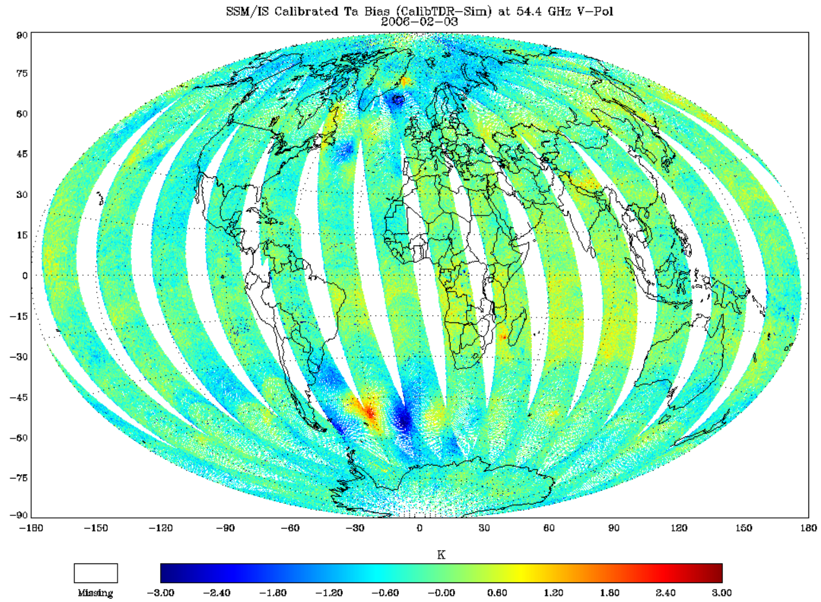

Corrected Ch 4 OB-BK (GDAS CRTM)

Fast SSMIS Zeeman Splitting Absorption Model

Energy level splitting:

In the presence of an external magnetic field, each O2 energy level associated with the total angular momentum quantum number J is split into 2J+1 levels corresponding to the azimuthal quantum number M = -J, …, 0, …,J

Transition lines (Zeeman components) :

The selection rules permit transitions with $\Delta J = \pm 1$ and $\Delta M = 0, \pm 1$. For a change in J (i.e. J=3 to J=4, represented by 3^+), transitions with

- $\Delta M = 0$ are called π components,
- $\Delta M = 1$ are called σ+ components and
- $\Delta M = -1$ are called σ- components.

Polarization:

The three groups of Zeeman components also exhibit polarization effects with different characteristics. Radiation from these components received by a circularly polarized radiometer such as the SSMIS upper-air channels is a function of the magnetic field strength |**B**|, the angle θ_B between **B** and the wave propagation direction **k** as well as the state of atmosphere, not dependent on the azimuthal angle of **k** relative to **B**.

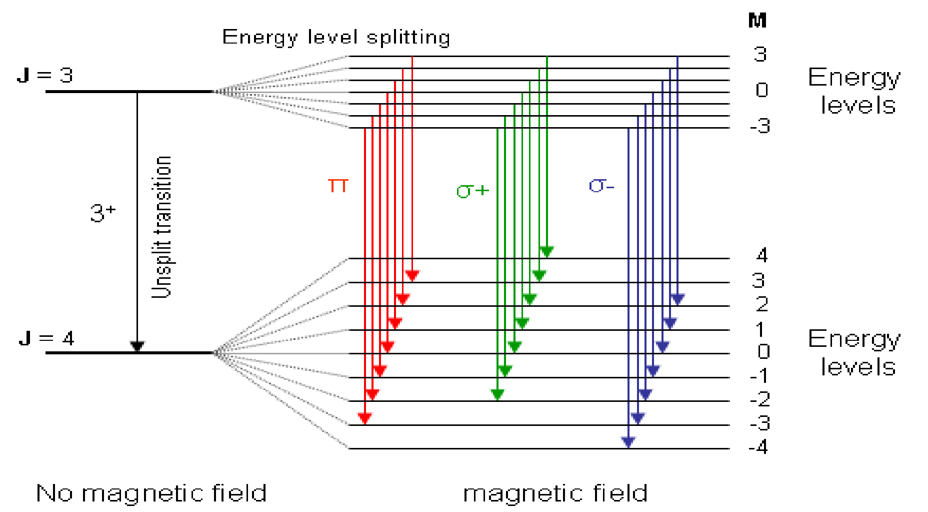

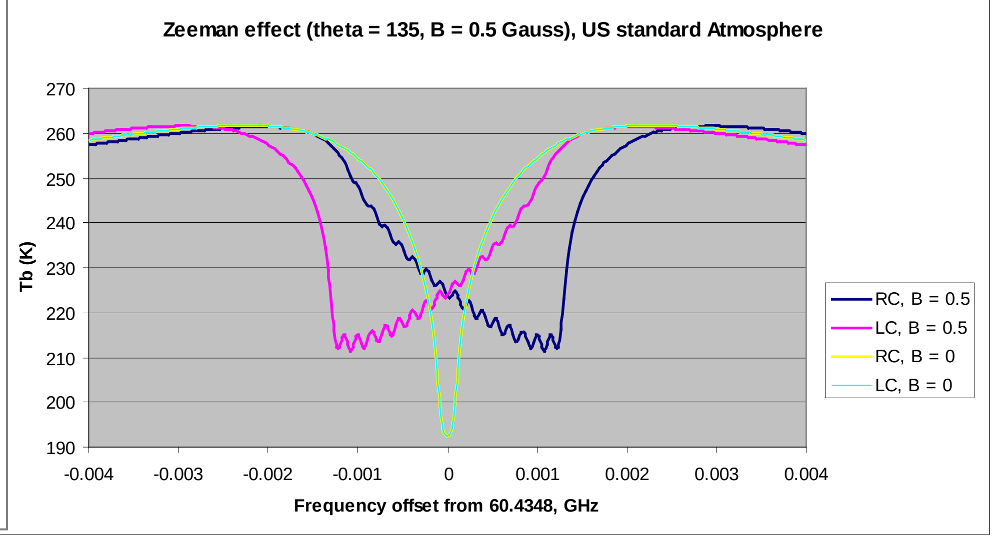

Comparison between SSMIS Observations and Simulations w/o Zeeman-effect

With Zeeman Effect

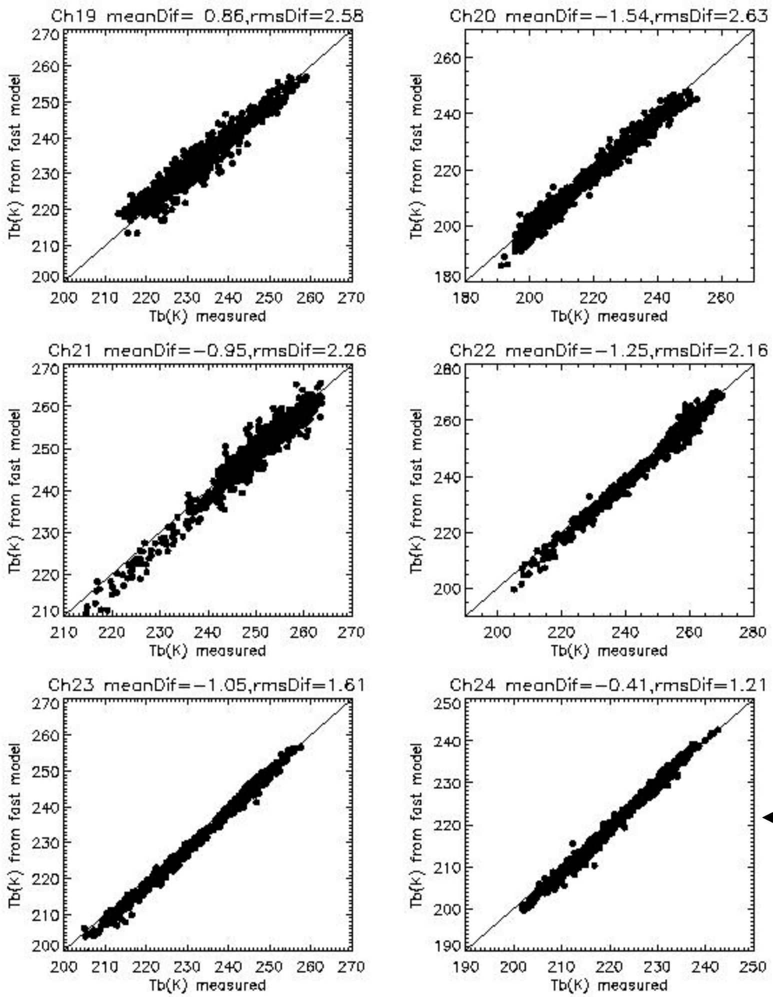

Without Zeeman Effect

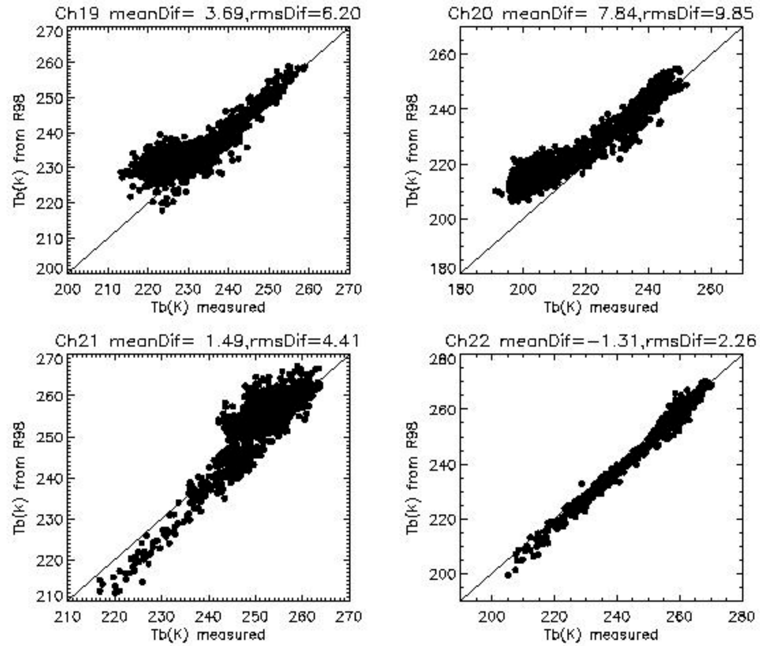

Without including Zeeman-effect in the model.

←Channels 23 & 24 are not affected by Zeeman-splitting

Collocated temperature profiles for model input are retrievals form the SABER experiment.

Sample size: 1097 samples

SSMIS Upper Atmospheric Sounding Channels

Before anomaly correction

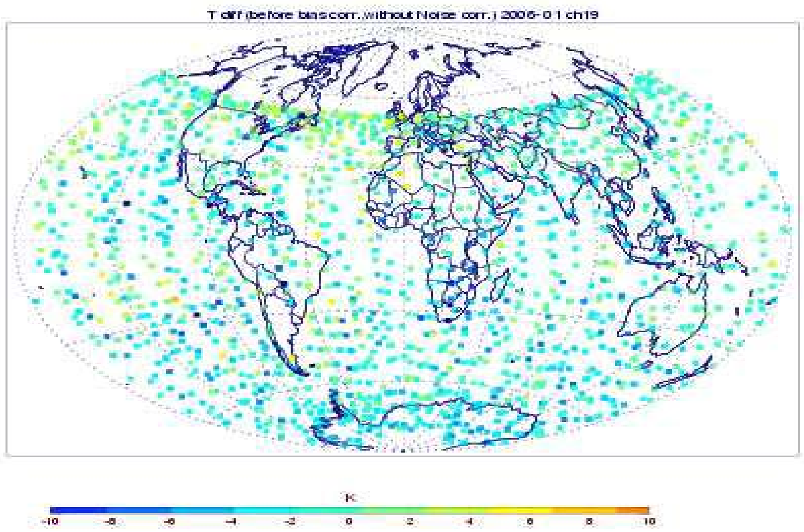

No correction TB(OBS) – TB(BK) at Ch. 19

After anomaly correction

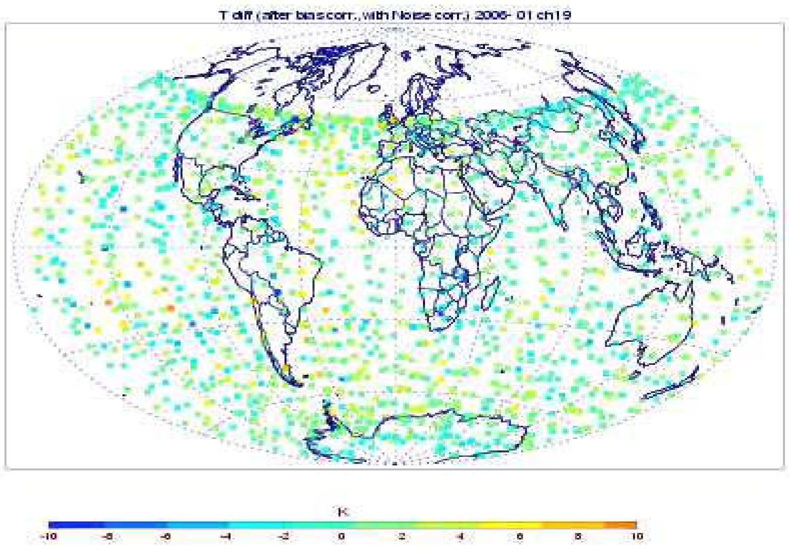

Correction TB(OBS) – TB(BK) at ch. 19

SSMIS UAS Correction

Before Bias Correction

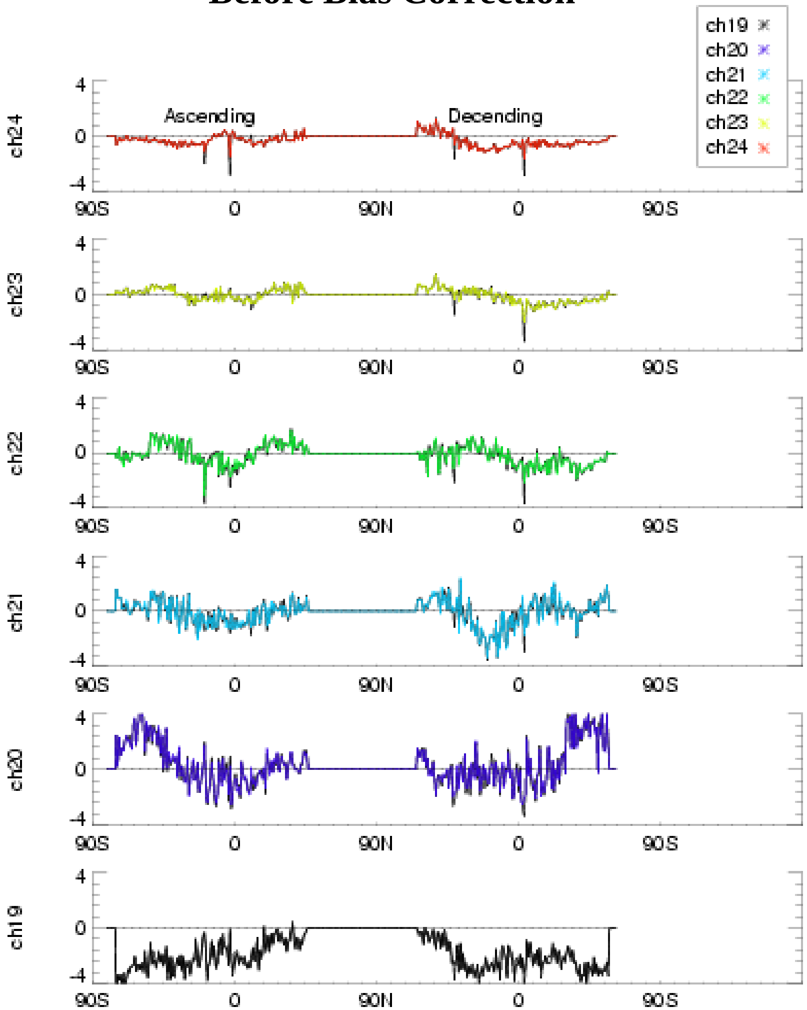

After Bias Correction

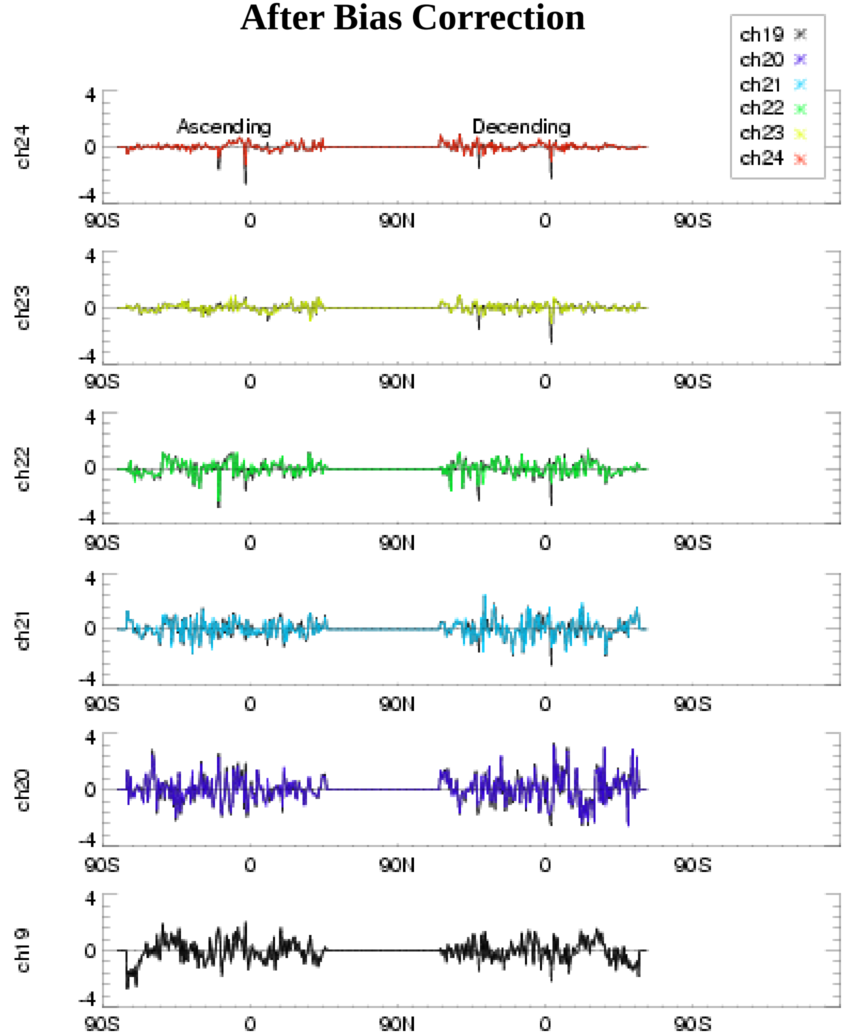

SSMIS LAS Radiance Assimilation in WRF

DMSP F-16 SSMIS radiances is at the first time assimilated using NCEP 3Dvar data analysis. The new data assimilation improves the analysis of surface minimum pressure and temperature fields for Hurricane Katrina. Also, Hurricane 48-hour forecast of hurricane minimum pressure and maximum wind speed was significantly improved from WRF model

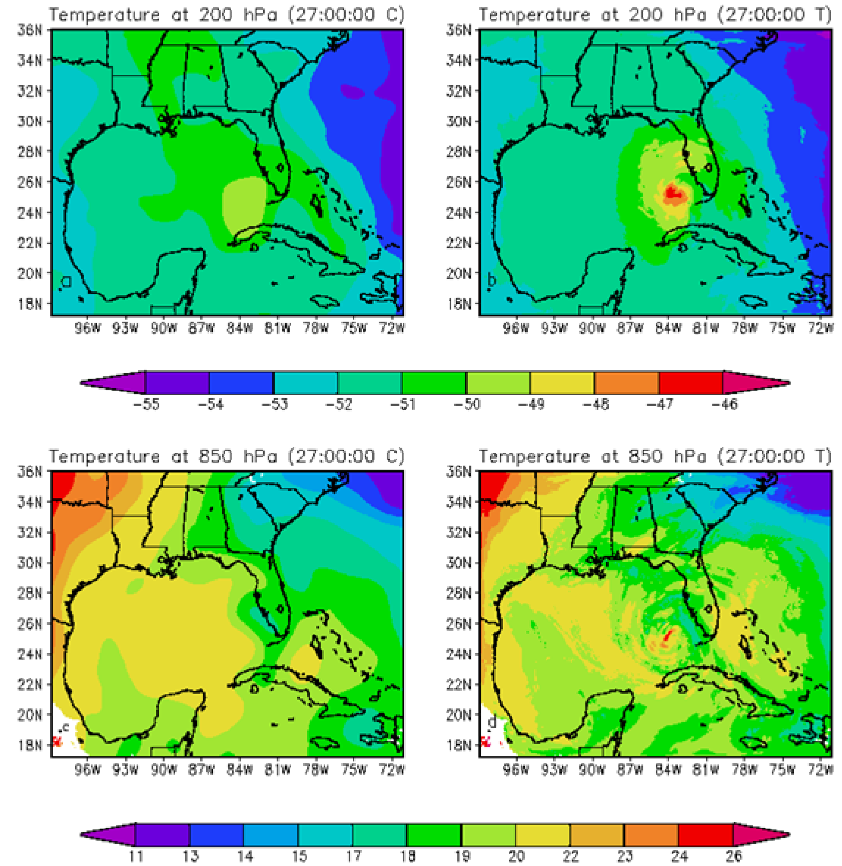

Significance: Direct assimilation of satellite radiances under all weather conditions is a central task for Joint Center for Satellite Data Assimilation (JCSDA) and other NWP centers. With the newly released JCSDA Community Radiative Transfer Model (CRTM), the JCSDA and their partners will be benefited for assimilating more satellite radiances in global and mesoscale forecasting systems and can improve the severe storm forecasts in the next decade

The initial temperature field from control run (left panels) w/o uses of SSMIS rain-affected radiances and test run (right panels) using SSMIS rain-affected radiances

Liu and Weng, GRL, 2007

Katrina Warm Core Evolution through NCEP GSI Analysis

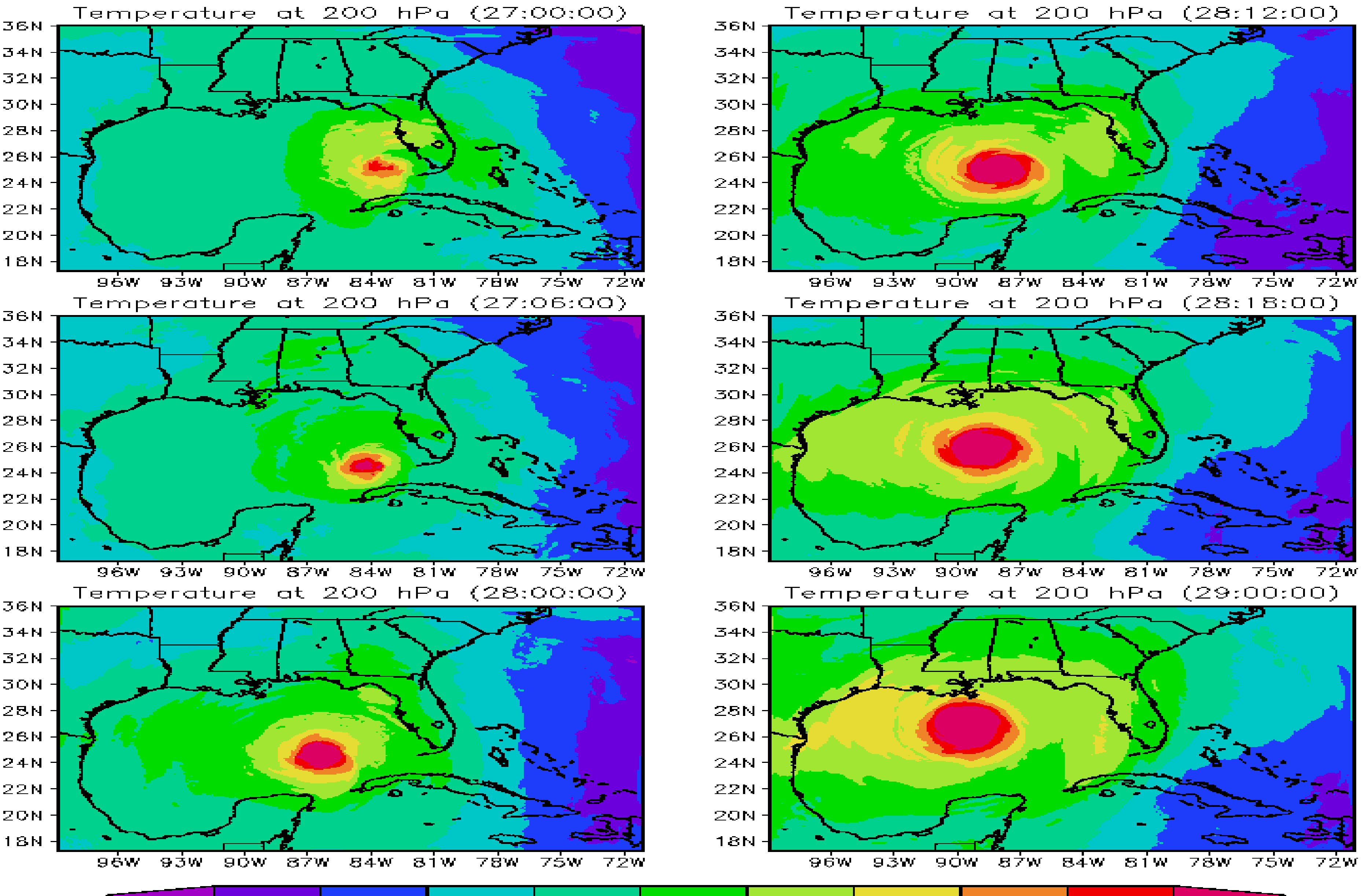

Summary and Conclusions

- The noise of Suomi NPP ATMS antenna temperature data is well characterized and meets the specification. The instrument performance is stable and produce the data for user applications

- ATMS TDR biases at the temperature sounding channels with respect to NWP simulations are uniform over the global conditions. The biases also display some angular dependence but smaller than those from AMSU-A. This dependence could be related to near-field side-lobe effects from satellites

- The effects of the NWP model top on the ATMS biases are well understood. To fully utilize the ATMS sounding capabilities, NWP model top must be set to 0.1hPa or higher.

- To derive ATMS SDR products, the conversion from a single polarization measurement may become non-unique for some sounding channels (e.g. channel 16) due to a larger cross-polarization spill-over effect

- DMSP SSMIS TDR data display strong latitudinal-dependent O-B. This dependence is related to the emitting antenna. Three SSMIS instruments all have similar anomalous features. Uses of TDR data in NWP systems need a careful bias corrections scheme.

- There are some other calibration anomalies in SSMIS sounding systems related to the warm load temperature and counts.